Synthesis and Spectroscopy of Silver-Doped PbSe Quantum Dots

Daniel M. Kroupa,[1,2‡] Barbara K. Hughes,[1,2‡] Elisa M. Miller,[1] David T. Moore[1], Nicholas C. Anderson,[1] Boris D. Chernomordik,[1] Arthur J. Nozik,[1,2] and Matthew C. Beard[1*]

1. Chemistry & Nanoscience Center, National Renewable Energy Laboratory, Golden, Colorado 80401, United States.
2. Department of Chemistry and Biochemistry, University of Colorado, Boulder, Colorado 80309, United States.

▪ *Abstract*

Electronic impurity doping of bulk semiconductors is an essential component of semiconductor science and technology. Yet there are only a handful of studies demonstrating control of electronic impurities in semiconductor nanocrystals. Here, we studied electronic impurity doping of colloidal PbSe quantum dots (QDs) using a postsynthetic cation exchange reaction in which Pb^{2+} cations are exchanged for Ag^+ cations. We found that varying the concentration of dopant ions exposed to the as-synthesized PbSe QDs controls the extent of exchange. The electronic impurity doped QDs exhibit the fundamental spectroscopic signatures associated with injecting a free charge carrier into a QD under equilibrium conditions, including a bleach of the first exciton transition and the appearance of a quantum-confined, low-energy intraband absorption feature. Photoelectron spectroscopy confirms that Ag^+ acts as a p-type dopant for PbSe QDs and infrared spectroscopy is consistent with $k \cdot p$ calculations of the size-dependent intraband transition energy. We find that to bleach the first exciton transition by an average of 1 carrier per QD requires that approximately 10% of the Pb^{2+} be replaced by Ag^+. We hypothesize that the majority of incorporated Ag^+ remains at the QD surface and does not interact with the core electronic states of the QD. Instead, the excess Ag^+ at the surface promotes the incorporation of < 1% Ag^+ into the QD core where it causes p-type doping behavior.

▪ *Introduction*

The intentional introduction of impurity atoms that inject free charge carriers into the electronic bands of a host semiconductor at equilibrium, also known as electronic impurity doping, has been essential to the growth and development of semiconductor based technologies including energy technologies such as solar cells, LEDs, and thermoelectrics.[1] Ideally, doping does not modify the electronic or physical structure of a semiconductor, but only changes its ability to conduct electrons or holes (negative or positive charge). In a bulk semiconductor, addition of impurity atoms can result in a shallow donor level below the conduction band and when ionized leads to a shift of the Fermi level towards the conduction band, producing an n-type semiconductor. Ionization of the semiconductor to a shallow acceptor level above the valence band, on the other hand, can shift the Fermi-level towards the valence band, producing a p-type semiconductor. Traditional methods of electronic impurity doping bulk semiconductors, including Si and GaAs, involve techniques such as growth addition, high temperature ion diffusion, and ion implantation. Despite much effort, reliable methods for controlling impurity doping within quantum-confined semiconductors are not readily available for a large range of semiconductor nanocrystal systems.

To date, there are four established methods used to inject free charge carriers or dopants into semiconductor nanocrystals, specifically quantum dots (QDs). The first method is remote chemical doping in which a molecule adsorbed to the QD surface undergoes redox chemistry to either inject (n-type) or withdraw (p-type) electron density. Remote chemical doping has been observed for PbSe QD films exposed to buffer solutions containing the ferrocene/ferrocenium redox pair rendering films p-type,[2] while exposure of PbSe QDs to cobaltocene leads to n-type doping.[3] Additionally, n-type doping of CdSe, CdS, and ZnO QDs has been observed upon addition of sodium biphenyl to QD solutions.[4] Another method of nanocrystal doping is through photochemical methods. Here, photogenerated carriers are 'captured' or 'quenched' by chemical oxidizers/reductants that strand the remaining photogenerated carrier, which is charge balanced by a surface counter ion. A prime example of photochemical doping is the generation of n-type CdSe QDs through photochemical oxidation of lithium triethylborohydride to scavenge photoexcited holes.[5] The third method of doping, electrochemical doping, is achieved through the application of an electrochemical potential to QD films. This method has been applied to samples of PbSe,[6] CdSe,[7] and HgTe[8] QDs. All three of these methods of QD doping are temporary and/or impractical for optoelectronic device fabrication where a fixed p-n junction is desired in order to direct the flow of charge carriers; however, these doping techniques allow for clean spectroscopic measurements of doped QDs that provide clear optical signatures of what should be observed upon successful QD electronic impurity incorporation including i) a bleach of the first exciton transition due to $1S_e/1S_h$ state filling (or Pauli-blocking) and ii) the appearance of a quantum-confined, low-energy intraband absorption feature arising from the $1S_e$-$1P_e$ transition for n-type doping or conversely from the $1S_h$-$1P_h$ transition for p-type doping.[9] Other spectroscopic observations of doped QDs include a decrease in the photoluminescence quantum yield (PL QY) with increased dopant incorporation and charged trion Auger decay of photoexcited excitons observed in time-resolved measurements.[5]

The final method of QD doping is conventional electronic impurity doping, which has been difficult to achieve in semiconductor nanocrystal material systems.[9] In fact, early assessments claimed that nanocrystals were "undopable" due to a thermodynamically-controlled selfpurification mechanism in which embedded impurity atoms are expelled or incoming impurity atoms rejected from the nanocrystal lattice in order to minimize the free energy of the nanocrystalline structure.[10,11] Furthermore, the electronic impurity atom/ion solubility limit is often exceeded in small nanocrystals. For example, 1 Ag atom in a 2 nm PbSe QD results in an impurity concentration of ~ 1%, which is near or above the solubility limit of Ag substituting for Pb in bulk PbSe.[12]

Electronic impurity doping involves the addition of impurity atoms (typically aliovalent) either substitutionally or interstitially into the QD lattice. There are at least four approaches towards QD electronic impurity doping: single source precursors, nucleation doping, surface treatments, and cation exchange.[13] We find cation exchange to be an advantageous approach seeing as doping levels can be easily controlled by altering dopant precursor concentrations. Additionally, cation exchange is a postsynthetic modification such that undoped QDs can be directly compared to subsequently doped QD samples. There have been numerous groups that have reported electronic impurity doping of QDs *via* cation exchange;[14–18] however, it remains unclear whether or not excess free carrier populations are present in these samples at equilibrium conditions due to the lack of data showing the spectroscopic signatures of electronic impurity doping – namely the lack of a reported first exciton transition bleach accompanied by a concurrent growth of an intraband transition observed with increasing dopant levels. In a recent review article, Schimpf *et al*. suggested that some of the observations reported in the literature could be attributed to a shift in the redox-potential of the cation exchanged QDs rather than conventional electronic impurity doping.[9]

In this study, we report electronic impurity doping of PbSe QDs using Ag^+ cations (Ag:PbSe QDs) and describe the changes to QD optical and electronic properties upon Ag^+ incorporation. First, we studied the efficiency of Ag^+ incorporation into the QDs. Subsequent absorbance measurements show a characteristic bleach of the first exciton transition when Ag^+ cations are incorporated and a concurrent size-dependent, low-energy absorbance, which we attribute to the intraband transition seen previously in remotely-, photochemically-, and electrochemically-doped QD samples. Photoelectron spectroscopy confirms theoretical predictions and previous experimental evidence that substitutional Ag^+ acts as a p-type dopant in PbSe, and further spectroscopic characterization provides additional evidence for electronic impurity doping.

▪ ***Results***

A. Cation Exchange Reaction and Physical Characterization

PbSe QDs were doped with Ag$^+$ *via* a partial cation exchange reaction from as-synthesized PbSe QDs using a procedure adapted from Norris and coworkers.[16] Experimental details are described in the Materials and Methods section. The concentration of Ag$^+$ dopant atoms exposed to the as-synthesized QDs was based on an estimation of the total starting Pb content per QD, but the final dopant incorporation was measured using analytical techniques. All labeling of Ag:PbSe QDs throughout this work will be reported as the Ag$^+$ content incorporated into the QDs based on the trends determined from elemental analysis.

TEM images shown in Fig. 1(A) and 1(B) indicate increased particle aggregation with increasing Ag$^+$ incorporation, but passing Ag:PbSe QD solutions through a 0.2 µm PTFE filter removed the largest insoluble aggregates.

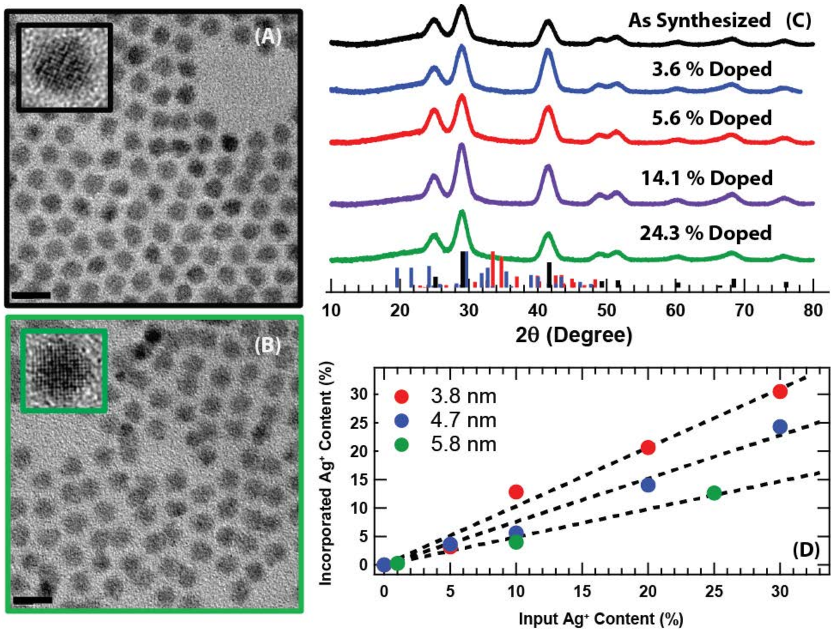

Figure 1. Characterization of the as-synthesized and Ag-doped PbSe QDs. TEM images show slightly increased QD aggregation with increasing dopant levels for (A) as synthesized and (B) 24.3 % doped 4.7 nm Ag:PbSe QDs. Scale bars are 10 nm. Insets show high-resolution TEM images. (C) XRD patterns of 4.7 nm Ag:PbSe QD samples. Stick diagrams for PbSe (black), Ag_2Se (red), and $AgNO_3$ (blue) are included for reference. (D) Elemental analysis data showing the amount of Ag$^+$ atoms incorporated into the Ag:PbSe QDs relative to the amount of Ag$^+$ added to the exchange solution.

We measured X-ray diffraction (XRD) for thin films of PbSe QDs and Ag:PbSe QDs containing 3.6% to 24.3% incorporated Ag$^+$ and find that the dopants do not fundamentally alter the crystal structure of PbSe QDs. The XRD patterns shown in Fig. 1(C) confirm that upon exchange the Ag:PbSe QDs retain the PbSe rocksalt crystallographic structure. Furthermore, there are no signatures of residual crystalline $AgNO_3$ or Ag_2Se in either the tetrahedral or orthorhombic phases (see Fig. S1 for a log plot). A high-resolution XRD scan with a reference was collected for the undoped and 30% input Ag^+ samples (see Fig. S2 for plot and deconvolution, Table S1 tabulates the peak positions). We find that the peaks are all slightly shifted for the doped sample, which is consistent with Ag^+ incorporation into the PbSe lattice.[12] We discuss the implications of the observed shifts in the discussion section. Elemental analysis, specifically X-ray fluorescence (XRF) or inductively-coupled mass spectrometry (ICP-MS), reveal that the incorporation of Ag^+ ions in the Ag:PbSe QD samples after purification is size-dependent where Ag^+ more easily incorporates into smaller QDs (Fig. 1(D)). This could be a result of improved Ag^+ binding to the PbSe QD $\langle 111 \rangle$ facets, which are more pronounced in PbSe QDs with smaller diameters,[19] or simply related to the larger surface-to-volume ratio.

Our results are in contradiction to those reported by Norris and co-workers. In order to efficiently incorporate Ag^+ into the lattice of a PbSe QD, they found that more Ag^+ needs to be added to the exchange solution than found here. In fact, they could only detect incorporated Ag^+ after addition of $AgNO_3$ concentrations that were greater than 50 – 100% of the total estimated Pb content in the QD sample. For 5.1 nm PbSe QDs with approximately 200% (Ag^+:Pb^{2+}) addition, they detected about 25 Ag^+ ions per QD. In contrast, we find that Ag^+ incorporates into the QD much more efficiently. For example, the ratio of input Ag^+ to incorporated Ag^+ is approximately 2 for 4.7 nm PbSe QDs, that is, 10 % (Ag^+:Pb^{2+}) input produces 5 % (Ag^+:Pb^{2+}) incorporation. Additionally, Norris and co-workers find the opposite trend of Ag^+ incorporation with respect to QD size. For their procedure, the incorporation of Ag^+ into PbSe was easier for larger QDs while we find it easier for smaller QDs. The major difference between the Norris procedure and ours is that they add trioctylphosphine (TOP) to the $AgNO_3$/ethanol solution to slow down the reaction so that a complete cation exchange does not occur. They found that TOP mediates the incorporation of Ag^+ into the PbSe QD lattice, but the addition of TOP must also modify the surface ligand interactions that mediate the cation exchange mechanism, ultimately producing a different Ag^+ incorporation trend with size. We have verified that adding TOP slows down Ag^+ incorporation into PbSe QDs in our laboratory, as well.

B. Cation incorporation mechanism

We propose that Ag^+ incorporation upon cation exchange is accomplished by a Z-type ligand exchange[20] at the QD surface in which $AgNO_3$ displaces $Pb(oleate)_2$. The removal of $Pb(oleate)_2$ is first suggested by the observation that the treated QDs tend to aggregate with increasing Ag^+

incorporation levels (Fig. 1A,B). We used quantitative ^{1}H NMR to better measure how the QD ligand surface coverage changed with increased Ag$^+$ incorporation. Experimental details and ^{1}H NMR spectra are described in the Materials and Methods section and Fig. S3, respectively. The broad vinyl proton peak of surface-bound oleate located between 5.0 – 5.5 ppm is well separated from the other peaks in the ^{1}H NMR spectrum, which makes it a useful indicator for quantitative experiments. We used ferrocene as an internal standard due to its high purity, ease of standardization in solution using absorbance spectroscopy, and sharp ^{1}H NMR peak near 4.2 ppm in $CDCl_3$, which is well separated from oleate peaks.

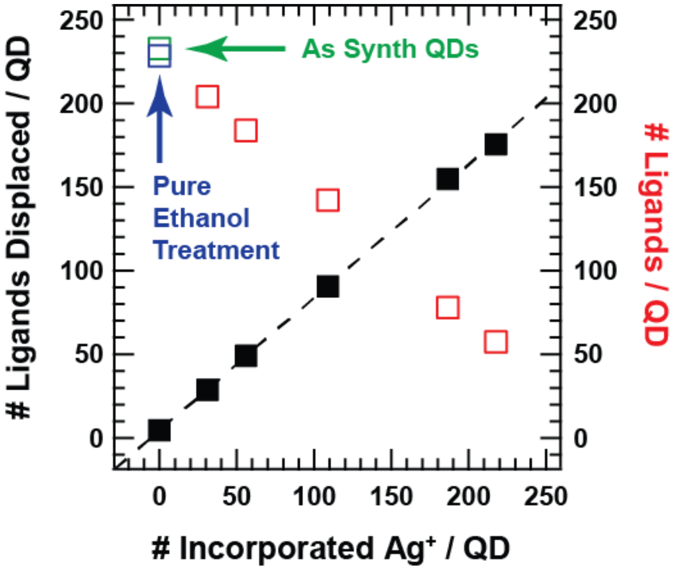

Figure 2. Summary of quantitative ^{1}H NMR spectroscopy experiments performed on 4.7nm PbSe QDs in $CDCl_3$. The number of bound oleate ligands per QD decreases as QD Ag$^+$ content increases suggesting a ligand-mediated cation exchange mechanism. The red squares represent the number of ligands per QD while the black squares are the number of ligands displaced per QD for the various Ag:PbSe QDs. The green point represents the as-synthesized QDs without any treatments, and the blue point represents PbSe QDs that were exposed to a similar volume of neat ethanol as those that are doped.

By determining the concentration of oleate in a given sample from ^{1}H NMR spectroscopy and the concentration of QDs from absorbance spectroscopy,[21] we are able to calculate the average number of ligands bound to a single QD. An initial concern was that ethanol exposure from the dopant precursor solution, which is known to displace oleate from the surface of metal chalcogenide QDs, was the cause for the observed aggregation.[22] However, a control experiment showed that QDs exposed to neat ethanol only resulted in the loss of ~ 4 ligands / QD, or 2% of the total oleate ligand coverage (Fig. 2, open green and blue squares). Combined with elemental analysis for the various Ag:PbSe QD samples, we were able to determine how the ligand coverage changes with Ag$^+$ incorporation (Fig. 2, open red squares). Within the error of the experiment and assuming a spherical, stoichiometric QD model, we found that for every

Ag^+ incorporated, approximately 1 oleate ligand was displaced from the surface of the QD (Fig. 2, solid black squares). Using this 1:1 ratio as a simple mechanistic guide, we conceive of two distinct schemes in which Ag^+ could be incorporated into a PbSe QD:

Scheme 1

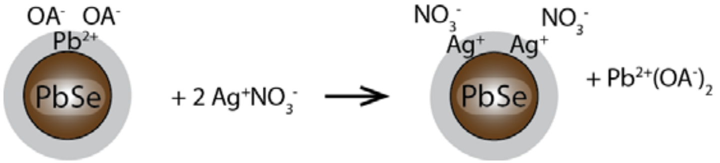

Scheme 2

In Scheme 1, a 1:1 exchange of Ag^+ for Pb^{2+} occurs with a single oleate ligand providing charge balance for the QD. Scheme 2 depicts a 2:1 replacement of Ag^+ for Pb^{2+}. In order to maintain an incorporated Ag^+: displaced oleate ligand ratio of 1:1, the QD in scheme 2 must be charge balanced by two NO_3^- ions. Both schemes are consistent with the data in Fig. 2 and can be classified as Z-type ligand exchanges.

C. Bleaching of Exciton Transitions

In order to determine the doping efficiency of Ag^+ cations in PbSe QDs, we measured the change in absorbance of the first exciton transition. As shown in Fig. 3(A), the sharp first and second excitonic absorbance features bleach with increasing Ag^+ content. It is also important to note that there is very little change in the peak position of the first exciton transition with increased Ag^+ incorporation, with a small red-shift for the highest doping level. Spectra are overlapped in the spectral region from ~1.6 eV to ~2.5 eV (Fig. S4) where the optical density should only be dependent on the amount of PbSe within the sample.[21] Control experiments were performed where neat ethanol, $Cd(NO_3)_2$, or $Pb(NO_3)_2$ was added to a QD solution in order to confirm that the observed bleaching was due primarily to Ag^+ incorporation (Fig. S5). We can estimate the average occupancy of delocalized carriers from the bleach of the absorption spectra assuming a Poisson distribution and an 8-fold degenerate $1S_e/1S_h$ exciton level. The normalized bleach is $\Delta\alpha/\alpha = \sum_{m=1}^{8} m \cdot P_m/8 + \sum_{m=9}^{\infty} P_m$, where $P_m = \langle N_p\rangle^m \; exp(-\langle N_p\rangle)/m!$ and $\langle N_p\rangle$ is the average number of delocalized dopants per QD. To determine $\Delta\alpha/\alpha$, we integrated the absorbance of the undoped and doped samples. For example, we find for the 4.7 nm diameter sample that $\langle N_p \rangle = 0.36, 0.87, 1.86$ and 2.49 for the 3.6%, 5.6%, 14.1%, and 24.3% doped samples (Fig. 3(B)). The slope of $\langle N_p \rangle$ vs % Ag$^+$ incorporated (Fig. 3B) is an estimate of the doping efficiency, and we find that about 10% Ag$^+$ incorporation leads to about 1 electronically active dopant per QD. Additionally, we found that the absorbance spectra of 4.7nm PbSe QDs with 24.3% Ag$^+$ incorporation exhibited nominal changes over 600 days of storage as a powder under inert atmosphere (nitrogen-filled glovebox) in the dark (Fig. S5(B)).

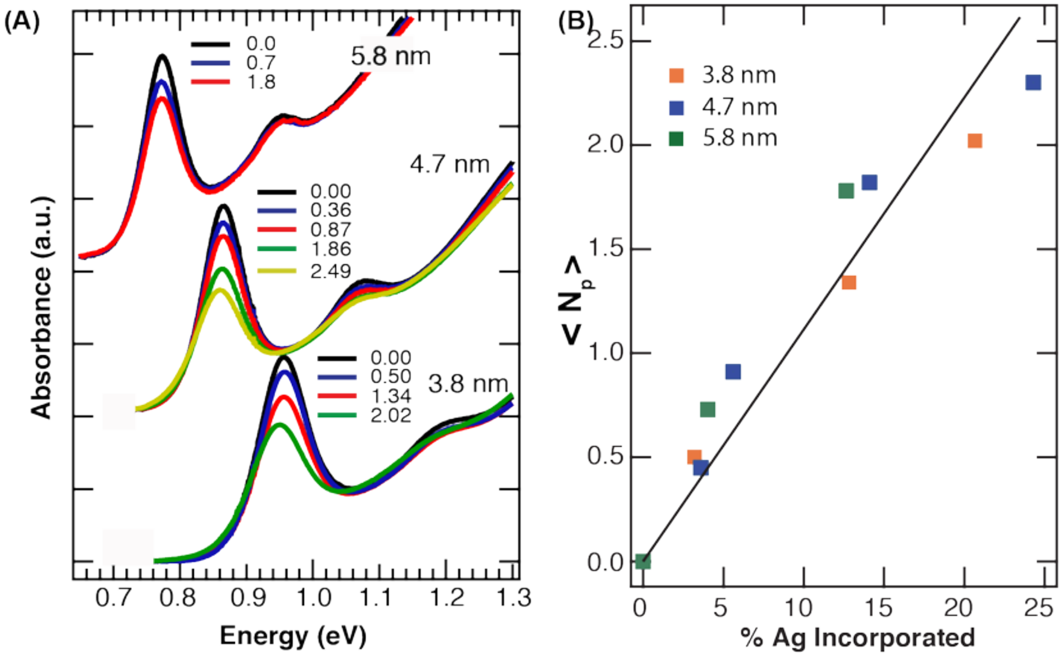

Figure 3. (A) Absorbance spectra of 3.8 nm, 4.7 nm, and 5.8 nm PbSe QDs dispersed in TCE as a function of the number of delocalized carriers, $\langle N_p \rangle$. The first and second excitonic features bleach with increasing dopant content due to band-edge state filling. The dopant percentage is determined from elemental analysis and $\langle N_p \rangle$ is calculated as described in the text (different colored traces). (B) $\langle N_p \rangle$ as a function of % Ag$^+$ incorporated gives a doping efficiency of 1 delocalized carrier per 10% Ag$^+$.

Calculations by Zunger and co-workers demonstrate that the first exciton transition strength can be modified either by charges present in interior states of the QDs or trapped charges at the surface of the QDs.[23] Charges injected into the interior PbSe QD states cause a reduction by Pauli-blocking (state-filling) resulting in a 1/8 reduction in oscillator strength for every 1 charge injected (assumed above). Trapped charges modify the absorption through electric field effects and result in both a shift of the energy levels (Stark shift) as well as a reduction in the oscillator strength. Thus, a bleach of the 1S exciton level alone is not sufficient to conclude that charges are present in the interior states of the QD. We do find that higher energy transitions (Fig. S4) show signs of both a small reduction in oscillator strength as well as shifted transitions, which we attribute to local electric fields at or near the QD surface. Also, the control experiments using $Cd(NO_3)_2$ and $Pb(NO_3)_2$ rather than $AgNO_3$ showed that the exciton transition can be slightly bleached and shifted (Fig. S5(A)), but the bleach is much less than observed for Ag^+ incorporation. We will use the intraband absorption along with the first exciton bleach data (see next section) to argue for charge present in interior states of the QDs.

D. Intraband Absorption

Previous studies using electrochemical, photochemical, and remote doping techniques have reported similar bleaching of the first exciton transition as that observed in this study. Those literature reports found that the first exciton bleach, when induced by doping, is accompanied by an absorption in the infrared corresponding to intraband transitions. The combination of these two observations (first exciton bleach / intraband transition) has recently been described as the spectroscopic signatures of excess band-like charge carriers upon QD doping.[9] The intraband absorption then arises from the excitation of these additional carriers from the $1S_e$ to $1P_e$ state for the case of an n-type dopant, or from the $1S_h$ to the $1P_h$ for a p-type dopant (schematic inset in Fig. 4A).

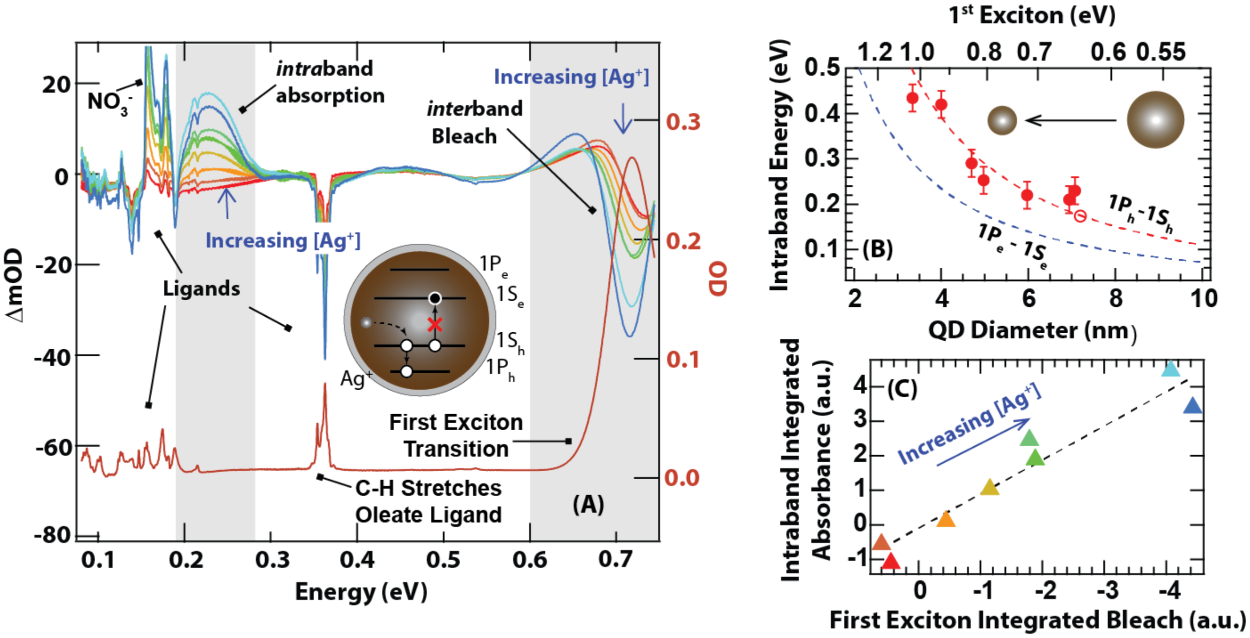

Figure 4. (A) FT-IR absorbance spectra of 6.0 nm EDT ligand exchanged PbSe QD films. The QD cartoon schematic represents the optical transitions expected for Ag:PbSe QDs. These optical signatures are observed in the differential FT-IR absorbance spectra and grow in/bleach as the PbSe QD film is exposed to increasing amounts of $AgNO_3$ in ethanol. The right axis corresponds to the red spectrum on the bottom showing a typical FT-IR absorbance spectrum of partially EDT-exchanged PbSe QDs. The left axis corresponds to the colored traces where negative values represent a bleach of the red spectrum and positive values represent a new absorbance peak. (B) Ag:PbSe QD intraband transition as a function of QD size (filled red circles) compared to calculated intraband energies from $k \cdot p$ theory (black dashed

line). Error bars represent the HWHM of the IR absorption band. The open red circle is the data point from Ref. [6] for the $1S_h$-$1P_h$ intraband transition measured using electrochemical doping. (C) Comparison of the integrated intraband absorption and first exciton bleach show a near linear dependence (black dotted line).

Accompanying the first exciton bleach, we observe an IR absorption band in Ag:PbSe QDs for all diameters studied here. The solid, red trace at the bottom of Fig. 4(A) shows the FT-IR absorbance spectrum of a thin film of 1,2-ethanedithiol (EDT) exchanged 6.0 nm PbSe QDs. We specifically chose to show this size QD sample so that both the exciton transition and the lower energy IR absorption band can be monitored simultaneously within our FT-IR spectral window. EDT treated films are employed so that the lower energy IR absorption band is not obscured by ligand-related IR bands. The colored traces at the top of panel 4(A) show the change in FT-IR absorbance (ΔOD) spectrum changes after exposure of the PbSe QD films to $AgNO_3$ in ethanol. For these measurements, the undoped film is used as the reference scan (red, bottom). Scans are then taken after exposure to $AgNO_3$ solutions for increasing amounts of time. The raw collected data is a difference scan, but an absorbance spectrum of Ag:PbSe QDs is reconstructed in Fig. S6. We found that increasing Ag^+ exposure, and thus QD incorporation, results in the appearance of a sharp infrared absorbance near 0.22 eV and a bleach of the first exciton transition near 0.72 eV. The intraband signal increases with increasing exposure to Ag^+ dopant solution, further emphasizing the Z-type ligand exchange mechanism discussed above. Furthermore, the structure to the red of the low energy transition is due to incorporated NO_3^- ions (presumably at the QD surface, see scheme 2).

The appearance of the IR absorption band could be attributed to (1) a localized surface plasmon resonance (LSPR) observed in heavily doped nanocrystals;[24] (2) the formation of small Ag_2Se nanocrystals (Ag_2Se is a small bandgap semiconductor);[25,26] and (3) an intraband absorbance induced by excess band-like charge carriers. We can rule out the LSPR because as the Ag^+ concentration increases, the center frequency and shape of the band does not change - only its intensity. As an example of how an LSPR behaves, Luther *et al*. showed a NIR LSPR resonance for copper deficient $Cu_{2-x}S$ particles (p-type) whose resonant frequency can be tuned by the dopant density. Such tuning of the resonance frequency is not observed here. Furthermore, the LSPR band is much broader than the IR absorption band observed here. We rule out the formation of Ag_2Se nanocrystals because no evidence is found in the XRD data of Fig. 1(C) or Fig. S1 that would suggest the presence of Ag_2Se domains. Saha *et al*. found that Ag_2Se nanocrystals with average diameter of 7.3 nm were required to achieve an exciton absorption centered near 0.22 eV[26] - much larger than the PbSe particles studied here and observed in TEM images. Finally, as shown in Fig. 4(B), the measured IR absorption band exhibits a QD size dependence consistent with $k \cdot p$ theory calculations for the $1S_h$-$1P_h$ transition (Calculations are detailed in Materials and Methods section).

To further rule out a reduction of the oscillator strength due to surface charging, we find that the first exciton transition bleaches in a linear fashion with the increase in intraband transition intensity for low doping levels (Fig. 4(C)). Note that the lowest doping levels (Fig. 4(A),(C)), red and dark orange traces) no intraband absorbance is observed and the change in 1st exciton absorbance can be attributed to a small shift of the band. Thus, we assign the IR absorption band as an intraband transition in the Ag:PbSe QDs and the bleach (Fig. 3) arises predominantly from state-filling rather than charges residing at the surface of the QDs. A diagram illustrating both the intraband absorbance and the first exciton bleach can be seen in the schematic of Fig. 4(A).

E. Photoelectron Spectroscopy

Ultraviolet photoelectron spectroscopy (UPS) and X-ray photoelectron spectroscopy (XPS) were performed on PbSe and Ag:PbSe QDs in order to determine how Ag^+ incorporation shifts the QD Fermi-level. For accurate XPS/UPS measurements of QDs, films must be conductive so that photocharging does not hinder data analysis. Here, we fabricate conductive films of PbSe and Ag:PbSe QDs *via* treatment with EDT to decrease inter-QD distance and displace the native ligand. Therefore, it is imperative to understand how the QD chemical environment can affect results. We know that as-synthesized PbSe QDs have an excess of Pb at the surface and tend to be n-type.[27] Subsequent treatment of QD films with EDT introduces surface chalcogen causing the QD Fermi level to shift towards the valence band edge (more p-type). Furthermore, we know that exposure of QDs to ambient conditions results in oxidation and also causes the QD Fermi level to shift towards the valence band edge (more p-type).[28] In this work, the QD films are kept strictly air-free to minimize oxidation (Fig. S7(A),(B)); thus, any observed changes in carrier type is a result of the added Ag^+ cations.

The UPS spectra for EDT exchanged films of the as synthesized, 3.6%, 5.6%, 14.1%, and 24.3% doped 4.7 nm diameter PbSe QDs are shown in Fig. 5(A) as solid lines. For a standard UPS or XPS analysis of the valence band maximum of semiconductors, the rise in photoelectron intensity nearest the Fermi energy (E_F) is usually assigned as the valence band maximum energy (E_{VBM}). To extract the E_{VBM} with respect to E_F ($E_F - E_{VBM}$), the rise in photoelectron intensity is fit to a line and extrapolated to a point that intersects a linear fit to the baseline (Fig. 5(A), dashed lines). In a recent report, Miller *et al*. demonstrated that a correction to the extracted onset of photoelectron intensity is needed to determine $E_F - E_{VBM}$ for PbS QD films due to a low density of states at the VBM (the onset of photoelectron signal is likely dominated by the Σ-valley and not the L-valley).[28] PbS and PbSe have similar energetic landscapes,[29] so we use the established correction for PbS here to better approximate the $E_F - E_{VBM}$ of the Ag:PbSe QD films studied here, as well. Note that the correction is a function of QD size and is a constant offset (181 mV for 4.7 nm QDs) to all extracted UPS and XPS photoelectron intensity onset values; therefore, the relative E_{VBM} trend would persist even without the correction.

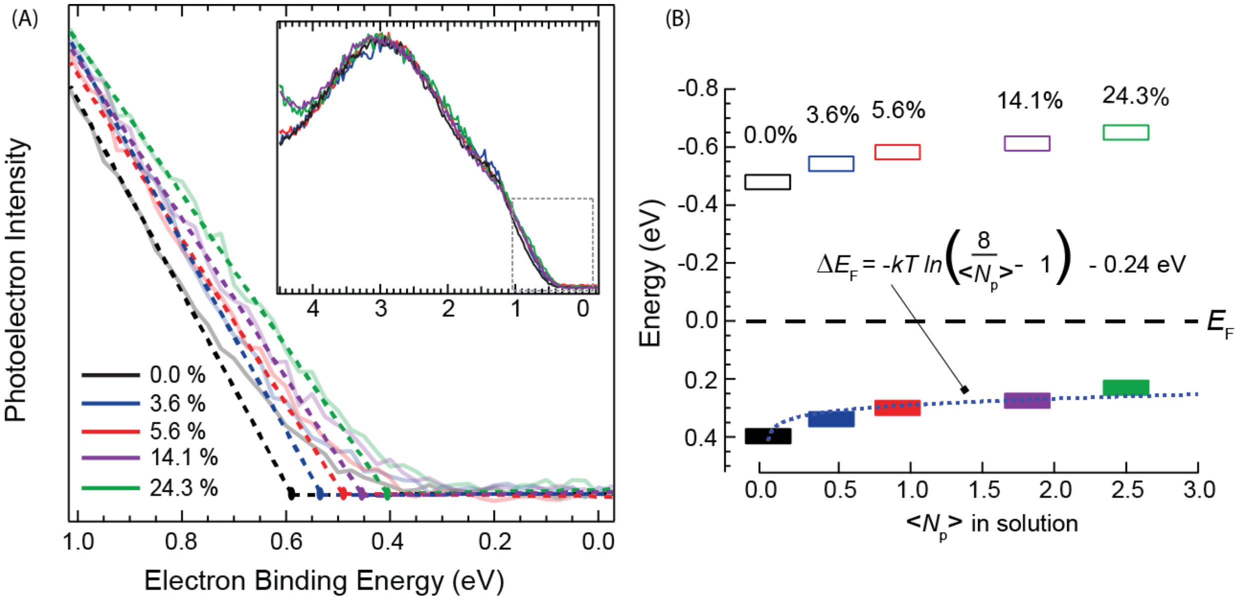

Figure 5. (A) UPS spectra showing the valence band edge region for EDT treated films of as synthesized (black), 3.6% Ag^+ doped (blue), 5.6% Ag^+ doped (red), 14.1% Ag^+ doped (purple), and 24.3% Ag^+ doped (green) 4.7 nm diameter PbSe QDs. The $E_F - E_{VBM}$ energies were extracted as described in the text, and shift to lower energies with increased Ag^+ content. (B) Corrected UPS band edge energies of PbSe QDs with respect to the Fermi level (set to zero). The closed and open rectangles represent the valence and conduction band edges, respectively. The conduction band edge was approximated by adding the band gap energy of respective colloidal samples measured using absorption spectroscopy plus the calculated exciton energy. The energy uncertainty of UPS measurements (±25 meV) is represented as the height of the rectangles. Overall, increasing the Ag^+ content in PbSe QDs results in more p-type character.

We find two clear trends from our data. First, both the UPS (Fig. 5(A) and Fig. S7(D)) and XPS (Fig. S7(C)) $E_F - E_{VBM}$ for Ag:PbSe QD films shift to lower electron binding energies as the Ag^+ content increases, indicating increasing p-type character with increased Ag^+ incorporation. This shift is consistent with Ag^+ acting as an electron acceptor (p-type dopant), which is expected if Ag^+ replaces Pb^{2+} in the PbSe QD lattice as a substitutional dopant (See discussion in SI). Second, there is a significant increase in the XPS and UPS photoelectron intensity around 5.5 eV with increasing Ag^+ content. This intensity is due to transitions from Ag 4d, which is consistent with the formation of Ag-Se bonds.[30] The fact that there is no photoelectron intensity at and below zero electron binding energy for both the XPS and UPS measurements suggests that Ag is incorporated as Ag^+ rather than Ag^0. The XPS/UPS results are summarized in Table S2. Note that the films were not measured in any particular order; therefore, the results are independent of time post-synthesis or any other systematic changes in the experimental setup.

The position of the Fermi-level relative to the valence band edge ($\Delta E_F = E_F - E_{VBM}$) upon doping for a PbS QD is $\Delta E_F = -kTln\big(8/\langle N_p\rangle - 1\big)$ since the $1S_h$ state is 8 fold degenerate. We find that the UPS and XPS data follows this trend (Fig. 5(B) shows results from UPS); however, a constant offset of -0.24 eV is necessary to fit the data, which indicates a per QD doping level within the films that is much lower than that of the isolated QDs in solution as determined from bleaching of the first exciton transition. The only significant difference between the QD films and QD solution samples is the presence of EDT at the QD surface for the film samples, which likely replaces the surface-bound NO_3^- and oleate anions of the solution samples. Thus, we suspect that EDT causes a de-doping of the QDs within the conductive films (this phenomenon is further discussed below).

F. Photoluminescence and Time-resolved Absorption Spectroscopy

The photoluminescence quantum yield (PL QY) was measured for 3.8 nm as synthesized and Ag:PbSe QD solution samples in TCE (Fig. 6). The introduction of additional Ag^+ impurities leads to quenching of the absolute PL QY of Ag:PbSe QDs, suggesting the introduction of new nonradiative relaxation pathways, consistent with previous reports.[5] If we assume that a doped QD does not emit, then the decrease in the PL QY corresponds to the number of delocalized dopants. For example, 3.2% Ag^+ incorporation corresponds to a doping level of $\langle N_p\rangle = 0.36$ and therefore ~ 60% of the QDs are not doped leading to ~ 40% reduction in the PL QY. Here, we observe a reduction of ~ 45%, which is in close agreement. We observe similar reductions in the PL QY for the other samples with increasing Ag^+ content, consistent with the $\langle N_p\rangle$ values determined from absorption bleaching. It is important to point out that the % Ag^+ incorporation is averaged over all QDs. Therefore, even though ~40% of the QDs register as doped, all of the QDs have ~3% Ag^+ incorporated. However, those QDs that are not electronically doped behave similar to QDs without any Ag^+ incorporated; thus, Ag^+ incorporation, by itself, does not modify the PL characteristics of the QDs, which is also consistent with the TA results discussed below.

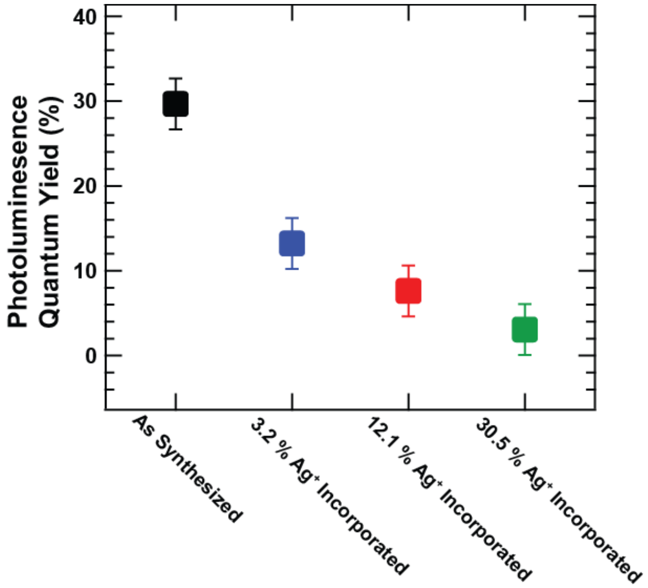

Figure 6. PL QY as a function of % Ag^+ incorporation for 3.8 nm PbSe QDs. The PL QY drastically decreases with increasing dopant levels, suggesting the addition of non-radiative recombination centers with increasing Ag^+ content.

We used transient absorption (TA) spectroscopy to capture both early (ps) and long (µs) exciton decay kinetics of 3.8 nm as synthesized and Ag:PbSe QD solution samples in TCE. Fig. 7 shows normalized TA kinetics for the various Ag:PbSe QD samples under identical laser excitation fluence. The laser pump wavelength was set to 700 nm, well below the multiple exciton generation (MEG) limit for these QD samples, and the pump fluence was adjusted to generate ~0.016 absorbed photons per pulse per QD, so no biexcitons are photoexcited during the experiment (the observed decay originates from single excitons only). As the Ag^+ dopant content increases, we observe a faster decay of the exciton population at delay times < 400 ns; but, the decay dynamics are identical at delays greater than ~ 400 ns.

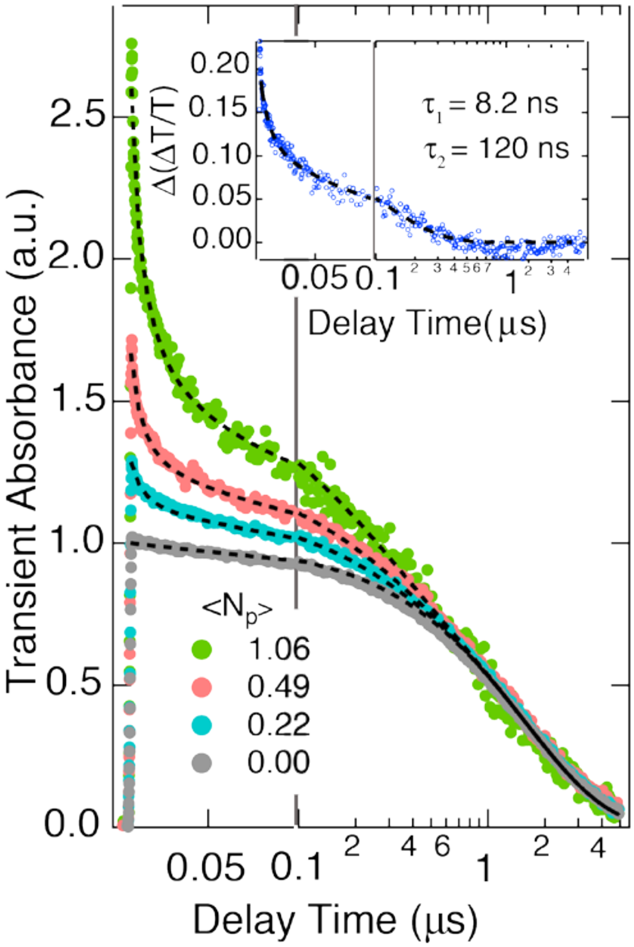

Figure 7. Decay dynamics of as synthesized and Ag:PbSe 3.8 nm QDs normalized by the amount of undoped sample. The undoped QDs have a single exponential lifetime of 1.55 µs. The dashed black traces are the results of the global model discussed in the text. The inset shows the response from just the electronically doped $\langle N_p \rangle = 0.22$ where the undoped response has been subtracted out; the response is biexponential with time constants of 8.2 ns and 120 ns.

To simulate the data, we ascribe the decreased exciton lifetime to the presence of electronic dopants. The data are first normalized so that the contribution to the decay from undoped QDs is equal to 1.0. For example, for the blue data in Fig. 7, the average number of dopants is determined from the bleach of the absorption to be $\langle N_p \rangle = 0.22$. Therefore, the fraction of the signal that arises from undoped QDs is $P_0 = 0.80$, and the data is then normalized so that its maximum is 1.25. Fig. 7 shows the normalized data for QDs with $\langle N_p \rangle = 0.00, 0.22, 0.49$ and 1.06. By normalizing in this fashion, the data at later times become coincident since the response from undoped QDs is normalized to 1.0. This implies that QDs that are electronically doped decay faster, while the longer delay time represents the exciton decay dynamics for only those QDs that are undoped. In order to model all of the transients from the differently doped samples, we first determine the kinetics of the undoped sample (Fig. 7, gray trace) and it can be represented by an exponential function with a time constant of 1.55 μs.

To determine the response from the doped QDs, we first took the difference between kinetics recorded for the sample with $\langle N_p \rangle = 0.22$ and the undoped sample, leaving only the kinetics from the doped QDs (inset of Fig. 7, blue points). We find that the dynamics of the doped samples cannot be represented by a single exponential function, but a double exponential decay can be used with best-fit time constants of 8.2 and 120 ns. All of the transients for the differently doped samples can now be modeled simultaneously using the following function:

$$\Delta\alpha(t)/\alpha = \sum_{m=0}^{\infty} \langle N_p \rangle^m / m! \cdot \varphi_m(t)$$

where $\varphi_m(t)$ is the response of QDs with m electronic dopants. We tested terms up to m = 5 but found that m = 2 is sufficient to completely reproduce the data set. In the global fit, φ_0 is a single exponential with a fixed time constant of 1.55 μs, φ_1 is a double exponential with time constants fixed at 8.2 and 120 ns as determined above, and φ_2 is a double exponential that is allowed to float. A global fit to the data was performed and the best-fit lines are shown as black dashed lines in Fig. 7, which find $\varphi_2$time constants of 2.7 ns and 50 ns.

▪ *Discussion*

Our data clearly demonstrates that we can achieve p-type electronic impurity doping of PbSe QDs through the incorporation of Ag^+, which gives rise to the spectroscopic signatures of QD doping. However, we observe two drastically different doping characteristics in PbSe QDs compared to bulk PbSe. First, the incorporated Ag^+ concentrations in our PbSe QDs (up to 30%) are much higher than the bulk solubility limit of Ag in bulk PbSe (between 0.5 and 1%).[12] From our XRD and TEM analysis (Fig. 1), we can conclude that Ag_2Se does not form as a separate component of the QDs. For example, Zhang *et al.* found that when Pb^{2+} is added to a CdSe QD, distinct PbSe components form with a well-defined XRD pattern, which can be readily observed in TEM pictographs;[31] however, this phenomenon is not seen here. Alternatively, an alloy would result in changes to the resulting crystal lattice constants,[32] which is also not observed in our XRD data. Additionally, in the bulk system, an alloy of PbSe and Ag_2Se does not form at low temperatures. Rather, they phase segregate for Ag^+ concentrations greater than ~ 1%.[33] Second, the measured doping efficiency for Ag^+ in PbSe QDs is much lower than Ag^+ in bulk PbSe. Specifically, Ag^+ doping of bulk PbSe is much more efficient needing only 0.1% Ag^+ incorporation to achieve hole carrier densities of ~ 1×10^{19} cm^{-3}.[12,34] In comparison, one delocalized carrier in a 4 nm diameter PbSe QD (~ 1000 total atoms with ~ 600 Pb^{2+} cations)[21] corresponds to a doping density of roughly $3x10^{19}$ cm^{-3} ($1/V_{QD}$). From elemental analysis, we can achieve close to 30% Ag^+ incorporation into PbSe QDs, which would give a doping density close to $5x10^{21}$ cm^{-3} ($180/V_{QD}$) assuming that all of the incorporated dopants are electronically active. This value would result in degenerately doped QDs, which is contradictory to what we observe from UPS, XPS, and absorbance measurements.

Taking these observations into consideration, we propose the following model to physically explain our data (Fig. 8). Most of the Ag^+ incorporation occurs at the carboxylate-passivated, metal-rich surface, which surrounds the stoichiometric QD core. For 3.8 nm diameter PbSe QDs, there is an excess of Pb^{2+} at the surface that amounts to ~ 30 – 40% of all Pb atoms.[35] Thus, Ag^+ replacement of the excess surface Pb^{2+} could result in up to a 40% Ag^+ incorporation with no apparent change in QD structural properties. Such a scenario is consistent with our observed Z-type ligand exchange. Furthermore, atomic ratios determined from XPS support the argument that Ag^+ replaces Pb^{2+}; the Pb:Se ratio decreases with Ag^+ incorporation (see Table S2 for atomic ratios). One might expect that if the Ag^+ forms a single layer at the surface then the 1S exciton energy level would shift to higher energies because the PbSe QD core would effectively shrink upon surface Pb^{2+} displacement; however, we do not observe a blue-shift. In contrast, when the concentration of incorporated Ag^+ is quite high (24%, corresponding to ~50% of the surface layer) a small red-shift is observed. To reconcile our observations, we conclude that the $Pb(oleate)_2$ ligand layer does not contribute significantly to the core first exciton state of the PbSe QD. This observation is consistent with the work of Anderson *et al.* within the metal chalcogenide QD system (CdSe and PbSe QDs). They found that displacing up to 80% of the metal carboxylate ligand shell resulted in only a small red-shift of the first exciton transition rather than the expected blue-shift corresponding to the shrinking of the QD core.[22] Thus, neither ligand exchange expressed in Scheme 1 and 2 is likely to provide electronic doping, as drawn, because the Ag^+ remains at the QD surface. Rather, the Ag^+ needs to diffuse into the lattice and substitutionally replace Pb^{2+} in the QD core for electronic doping to be realized.

The diffusivity of Ag^+ in bulk PbSe was found to be ~6×10^{-10} cm^2/s at room temperature.[36] Therefore, for a PbSe QD with diameter of approximately 4 nm, Ag^+ can diffuse across the length of the nanostructure in about 200 μs. Therefore, a Ag^+ cation within the PbSe QD core is more likely to diffuse out of the lattice and reside at the QD surface where it does not contribute to electronic doping. Thus, we propose that a reservoir of Ag^+ resides at the QD surface and establishes an equilibrium concentration of dissolved Ag^+ within the PbSe lattice of the QD core. In bulk PbSe, the addition of Ag^+ increases the diffusion of Pb^{2+} within the PbSe lattice, thereby lowering the activation energy of vacancy formation.[34] The diffusion of Ag^+

within the PbSe lattice mainly occurs through interstitial sites and promotes the formation of Pb^{2+} vacancy in order to substitute. The surface Ag^+ layer also electronically passivates

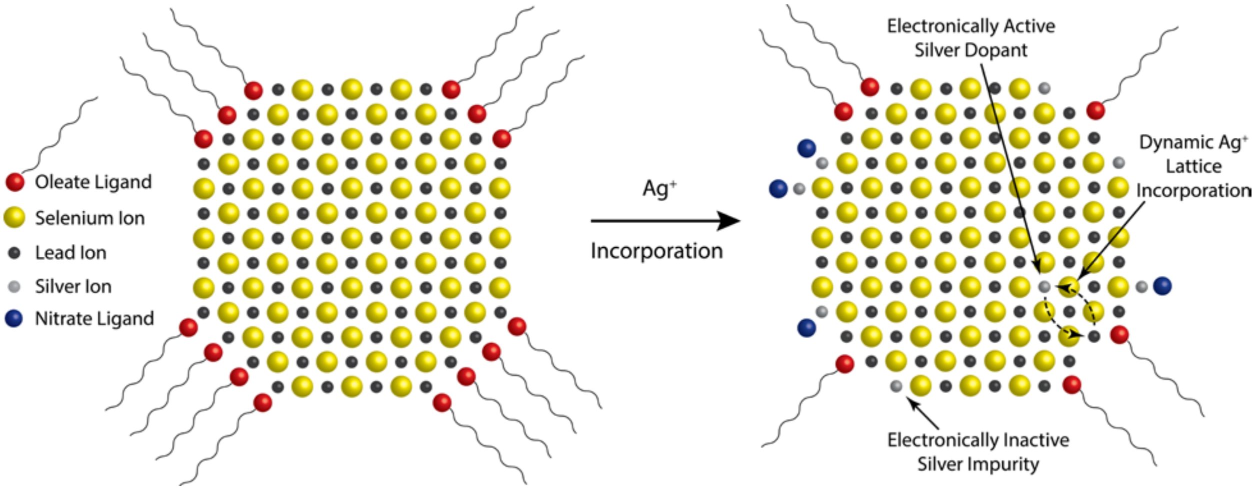

Figure 8. Simplified 2D schematic of the proposed doping scheme in Ag doped PbSe QDs. The left panel shows an undoped QD consisting of excess Pb along the {111} facet, where each excess Pb^{2+} cation is compensated by two oleate ligands (red sphere/black tails). The right panel shows the QD after incorporation of ~ 10% $AgNO_3$ through a mixture of scheme 1 and scheme 2 mechanisms. Most of the incorporated Ag^+ cations (grey spheres) reside within the electronically inactive ligand shell; some of the nitrate anions (blue spheres) remain. A large excess of Ag^+ residing at the shell can promote the substitution of Ag^+ for core Pb^{2+} (black spheres) resulting in p-type electronic doping. The equilibrium between surface and core Ag^+ depends upon the nature of the Ag-ligand bonding.

surface Se^{2-} anions as Z-type ligands similar to the original $Pb(oleate)_2$ surface layer.

Direct evidence for Ag^+ substitutional incorporation into the PbSe QD core at a lower percentage than the total incorporated Ag^+ as measured from elemental analysis can be found in high-resolution XRD data. Figure S2 shows the XRD peaks for the (220), (311), (222), (400), (420), and (422) reflections. Each of the peaks associated with the Ag:PbSe QDs shift by at least 0.05 degrees compared to the undoped PbSe QD sample. We show the (422) XRD peak for both the Ag:PbSe and undoped QD samples in Fig. 9 where the peak is shifted from 76.22 degrees for the undoped QD sample to 76.39 degrees for the Ag:PbSe QD sample. Wang *et. al.* studied Ag^+ incorporation in bulk PbSe and found that the PbSe lattice contracts with substitutional incorporation of Ag^+, resulting in the XRD reflection peaks shifting by at most 0.2 degrees for 2% Ag^+ incorporation (roughly consistent with Vegard's law).[12] Thus, our XRD data suggest that the amount of Ag^+ substitutionally incorporated into the PbSe lattice is less than 2%, even though the elemental analysis data suggest ~ 25% incorporation into the QD structure.

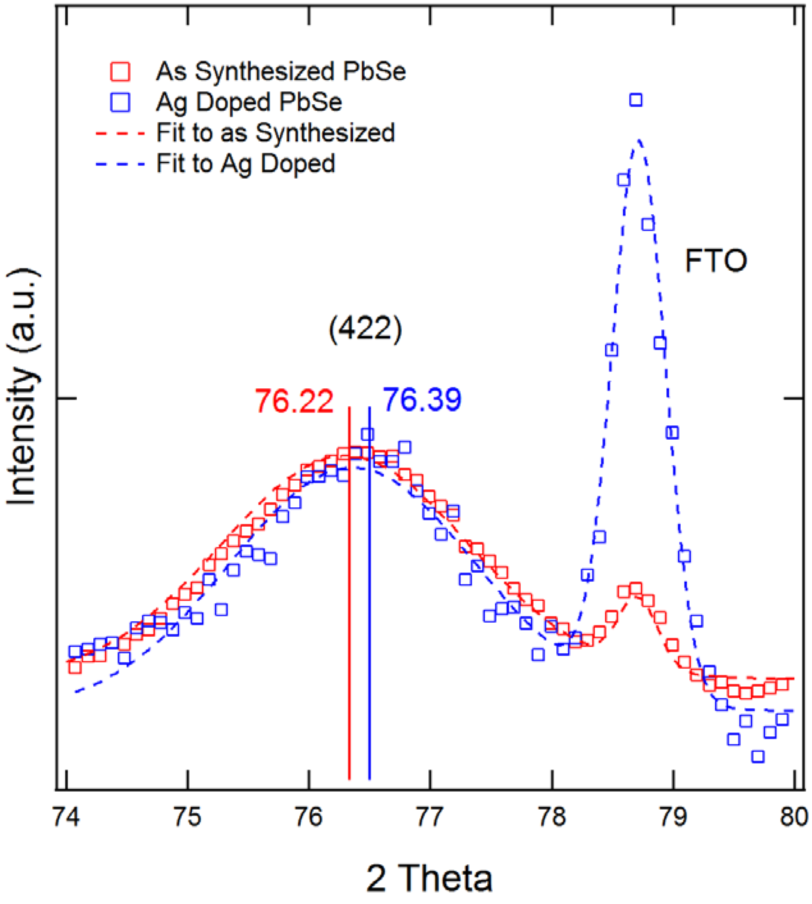

Figure 9. High resolution XRD comparison of doped and undoped PbSe QDs. The FTO substrate serves as a reference and deconvolution shows a shift of 0.17 degrees for the doped sample. (For the full spectra, see Fig. S2).

Our proposed doping model with a dynamic equilibrium between surface-bound and core-incorporated Ag^+ can also explain our photoelectron spectroscopy results. While the QDs are initially doped in solution with oleate and NO_3^- surface passivation, the ligands must be exchanged in order to render the films conductive for UPS/XPS measurements. For our experiments, we perform a ligand exchange to fabricate PbSe QD films using EDT, which presumably displaces oleate and NO_3^- yielding a thiol/thiolate surface passivation. According to the hard/soft acid base concept, Ag^+ and S^{2-} are a soft acid and a soft base, respectively, while NO_3^- is a hard base; thus, the Ag-sulfur bond is much stronger than the Ag-NO_3 interaction. We propose that the stronger Ag-S bond at the QD surface will shift the dynamic doping equilibrium towards electronically inactive surface-associated Ag^+ and effectively reduce the overall QD doping level. Our XPS/UPS valence band energetics suggest that the doping within EDT treated QD films is ~ $exp(-0.24/kT)$ or 10^4 less than in the isolated oleate and NO_3^- passivated QD solution samples. The doping density of a QD in solution with 1 active carrier is $3x10^{19}$ cm^{-3}, therefore, we estimate that the doping density of the EDT treated QD film to be on the order of ~ 10^{15}cm^{-3}; thus, the doping efficiency of Ag$^+$ in the EDT treated PbSe QDs is even less efficient, highlighting the fact that strategies to produce electronically doped QD films must also consider ligand-dopant interactions.

Our model is roughly consistent with that proposed by Amit *et.al.*[37] even though the chemical details are quite distinct. They studied Ag$^+$ doping of InAs QDs and found that at low concentrations of added Ag$^+$ that the cation incorporates into the InAs lattice, while at higher concentrations (above the solubility limit of Ag$^+$ in InAs) the additional Ag$^+$ is found at the surface of the QDs. We note that they achieve Ag$^+$ doped InAs QDs using $AgNO_3$, similar to the method described here; however, in their reaction, they use two additional reagents; N,N-di-*n*-dodecly-N,N-dimethylammonium bromide (DDAB) and *n*-dodeclyamine (DDA). These reagents stabilize the Ag$^+$ cation and also act as a reducing agent at elevated temperature. Therefore, the reduction of Ag$^+$ to Ag^0 can lead to chemical doping of the InAs QDs. In our reaction, we do not add a reducing agent and the reaction is performed at room temperature, but it is still conceivable that some small amount of Ag$^+$ is reduced by the QD to form Ag^0 and p-dope the sample. To test this possibility, we performed electron paramagnetic resonance (EPR) spectroscopy on the Ag:PbSe QD samples; however, in all measurements, we found no evidence for a Ag^0 signal above the background noise level (Experimental details can be found in the Materials and Methods section). Therefore, we discount this possible effect.

Intuitively, if Ag atoms (one valence electron) were to substitutionally replace Pb atoms (two valence electrons) in the PbSe lattice, Ag would dope the QD p-type, similar to Boron doping in Silicon. Theoretical calculations of bulk Ag:PbSe where Ag$^+$ substitutes for Pb^{2+} on the PbSe lattice shows the formation of an acceptor level that causes a lowering of the Fermi level (p-type doping),[38] which is likely what occurs in our Ag:PbSe QD system, as well. We illustrate this concept using molecular orbital (MO) theory of a simple 4-atom model. Figure 10(A) shows a simplified MO diagram of Pb_2Se_2, representing the electronic structure of an as-synthesized PbSe QD core. Taking into account s-p orbital interactions, the highest occupied molecular orbital (HOMO; valence band) arises from interactions between the Pb-s and Se-p states, and the lowest unoccupied molecular orbital (LUMO; conduction band) arises from interactions between the Se-s and Pb-p states. Figure 10(B) shows a simplified MO diagram of $AgPbSe_2$, representing the QD core when Ag is substituted for Pb. The Ag-related atomic orbitals of interest are the Ag-s and Ag-d orbitals, which both interact with the Se-p orbitals. Specifically, the Ag-s orbital introduces a bonding and antibonding state in the valence band and conduction band, respectively. In a cubic PbSe lattice, the five-fold degenerate Ag-d orbitals split into three lower energy T_1^d states and two E^d states due to splitting of the octahedral crystal field. The T_1^d states weakly couple with the Se-p states, but the E^d state couples more strongly, introducing antibonding states near the Pb-Se HOMO (valence band edge). In an atomic lattice with many PbSe units, these Ag-Se states form localized impurity states, which are thoroughly described in Ref. 38.

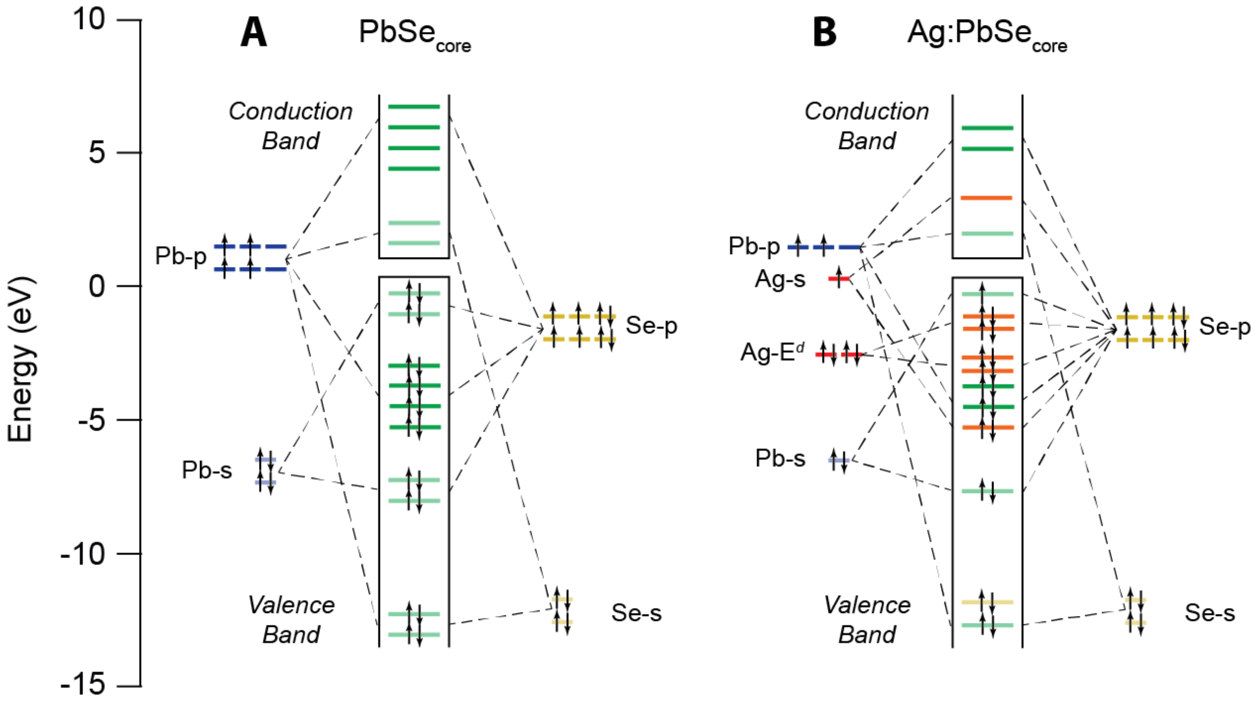

Figure 10. Orbital character of the band edge region in (A) PbSe and (B) Ag:PbSe QD cores. Blue orbitals are associated with Pb, yellow orbitals are associated with Se, and red traces are associated with Ag. Green states are composed of Pb and Se character, while orange states are composed of Ag and Se character.

Studies from the Norris group on CdSe QDs showed that Ag^+ acts as an n-type interstitial donor at low concentrations, but transitions to a p-type substitutional donor at higher dopant levels.[15] In bulk PbSe, the opposite appears to occur. At concentrations of less than 1%, Ag^+ dynamically substitutes for Pb^{2+} and behaves as a p-type dopant, while for concentrations greater than 1%, Ag^+ incorporates interstitially and behaves as an n-type dopant.[12] In the systems studied here, we are apparently unable to drive the incorporated Ag^+ concentration high enough to achieve interstitial doping of PbSe QDs in the solution phase, likely because increased Ag^+ incorporation is accompanied by further displacement of the carboxylate ligands causing the QDs to lose their colloidal stability.

Finally, we consider the effects of an electronic dopant on excited state lifetimes of PbSe QDs as measured using time-resolved TA spectroscopy. The introduction of an electronic dopant should decrease the exciton lifetime due to an increase in the number of recombination pathways. In addition, non-radiative Auger recombination pathways become possible and can drastically reduce the carrier lifetimes to be less than 1 ns. According to Klimov and co-workers, the trion lifetime should be related to the biexciton lifetime by $\tau_{A,N_d} = 8\tau_{A,xx}/[N_p(N_p+1)]$.[3] The kinetics of the as-synthesized QD sample shows a biexciton lifetime of 60.5 ps (not shown), which is consistent with previously measured PbSe QDs. Therefore, the trion lifetime should be ~ 242 ps, which is roughly the value Klimov and co-workers measured for PbSe QDs doped n-type through a charge transfer reaction from cobaltocene;[3] however, we find much different behavior. For the singly doped QDs we measured a biexponential decay with lifetimes of 8.2 and 120 ns - much longer that that predicted. The 120 ns is closer to a modification of the radiative lifetime $\tau_{r,N_d} = \tau_r/(N_p+1)$ or 775 ns. For QDs with two dopants, the lifetimes decrease by about half from 8.2 and 120 to 2.7 and 50 ns. A possible explanation, though not completely satisfactory, for the observed long lifetimes could be that Ag^+ passivation softens the potential at the QD surface. Such softened potentials have been shown to reduce the Auger recombination probability,[39,40] although, more work is needed in order to clarify the longer lifetimes that we observe.

▪ *Conclusions*

In this work, we demonstrate an effective method of incorporating Ag^+ cations into PbSe QDs using a postsynthetic cation exchange technique that does not significantly perturb the original PbSe QD crystalline matrix. We find that Ag^+ incorporation is accompanied by a Z-type ligand exchange at the QD surface where $Pb(oleate)_2$ is displaced by $AgNO_3$. Additionally, we observe the spectroscopic signatures of electronic impurity doping in QDs, specifically, a bleaching of the first exciton absorbance feature accompanied by the growth of a quantum confined infrared intraband absorbance. We also observe a quenching of band edge PL and the acceleration of a fast exciton decay channel with increasing Ag^+ incorporation suggesting the introduction of new, nonradiative relaxation pathways with increased doping. Using photoelectron spectroscopy, we unequivocally assign Ag^+ as a p-type dopant for PbSe QDs, which is consistent with previous Ag doping of bulk PbSe. We propose a model whereby the majority of the added Ag^+ remains at the QD surface and does not interact with the PbSe QD core electronic states. Small amounts of Ag^+ diffuse into the lattice and establish a dynamic equilibrium between electronically inactive surface-bound Ag^+ and electronically active lattice-incorporated Ag^+, which we propose can be tuned through the introduction of other surface coordinated species. The demonstration of a technique to controllably synthesize solution processable p-type semiconductor nanocrystals under equilibrium conditions will benefit numerous technological applications such as solar cells, photoelectrochemical cells, LEDs, and thermoelectrics.

- ***Materials & Methods***

A. Materials

All chemicals were used as received without further purification. Selenium (Se, 99.99%), oleic acid (90%), diphenylphosphine (DPP, 98%), trioctylphosphine (TOP, 90%), 1-octadecene (ODE, 90%), silver nitrate (99+%), cadmium nitrate tetrahydrate (trace metals basis, 99.999%), lead nitrate (trace metals basis, 99.999%), 1,2-ethanedithiol (EDT, ≥98%), anhydrous ethanol (EtOH, 200 proof, ≥99.5%), Nitric Acid (TraceSELECT®, ≥69.0%), ultrapure water (TraceSelect® Ultra), anhydrous hexane (≥99%), anhydrous acetonitrile (99.8%), anhydrous tetrachloroethylene (TCE, ≥99.9%), anhydrous chloroform-d ($CDCl_3$, ≥99.8%), and ferrocene (Cp_2Fe, 98%), were purchased from Aldrich and used as received. Lead oxide (PbO, 99.999%) was purchased from Alfa Aesar.

B. QD Synthesis and Purification

PbSe QDs were synthesized and purified using standard air-free techniques. In a typical synthesis, a solution of 1.015 g PbO, 4.008 g oleic acid, and 11.586 g ODE was degassed in a three-neck flask under vacuum and heated to 120°C for 1 hour. Fifteen milliliters of a 1 M solution of TOP-Se containing 0.15 g DPP was then rapidly injected into the hot Pb solution. The QDs were grown for 1-5 minutes, and the reaction was quenched with a water bath and injection of 20 mL of room temperature hexanes. The QDs were purified by three rounds of precipitation/centrifugation/redissolution purification using hexane and ethanol as the solvent and anti-solvent, respectively. The fully purified QDs were stored as a powder in a nitrogen filled glovebox in the dark.

C. Solution Doping of PbSe QDs

To estimate the electronically active Pb content of the stoichiometric PbSe QD cores, the QDs were treated as perfectly spherical and stoichiometric particles (which systematically underestimates the Pb content per QD since PbSe QDs have been shown to have a Pb-rich surface).[41] The total number of core Pb atoms per QD can be estimated by dividing the QD volume, $\frac{4}{3}\pi r^3$ where r is the QD radius determined from absorption spectroscopy and TEM imaging, by the volume of the PbSe rock salt unit cell, a^3, where a is the PbSe lattice constant, and multiplying by the number of Pb atoms per unit cell (4 atoms). The concentration of QDs per sample can be determined from absorption spectroscopy to then calculate the total number of lead atoms per sample.[21]

The necessary amount of silver(I) nitrate ($AgNO_3$, concentrations ranging 5-35% Ag:Pb) was dissolved in minimal ethanol and pipetted into room temperature, stirred solutions of PbSe QDs in hexane. The exchange was allowed to proceed for 10 mins at which time the reaction was quenched by precipitating the QDs from suspension with the addition of ethanol. Following exchange, the Ag:PbSe QDs were subjected to three consecutive cycles of precipitation, redissolution, and centrifugation purification cycles (PCR purification) to remove any excess $AgNO_3$ or displaced Pb-oleate related species free in solution. Specifically, the Ag:PbSe QDs were precipitated from suspension in hexane by the addition of an anti-solvent, ethanol. Next, the sample was centrifuged at 7500 RPM for 5 mins and the supernatant discarded. The Ag:PbSe QD pellet was then resuspended in hexane for further purification, or at the end of purification, was stored as a powder in a nitrogen filled glovebox in the dark. Ag:PbSe QD powders were resuspended in hexane for film formation or in tetrachloroethylene for optical characterization.

D. QD Film Preparation

a. XRD Analysis

Films were prepared for XRD by dropcasting undoped or solution doped Ag:PbSe QDs from hexane onto Si or FTO substrates.

b. XPS/UPS Analysis

Thin films were prepared for XPS/UPS analysis *via* a layer-by-layer spincoating technique. Undoped or solution doped Ag:PbSe QD solutions (~20 mg/mL in hexane or octane) were deposited onto Au/Cr coated glass substrates and spun at 2500 RPM for 30 s. The substrates were then submerged in 1 mM EDT acetonitrile solution for 30 s to replace the native oleate/nitrate ligands with EDT. This process was repeated for a total of four cycles to build up a sufficiently thick, conductive film for photoelectron spectroscopy.

c. FT-IR Analysis

In order to build up a sufficiently thick QD film in which the IR intraband can be detected using FT-IR transmission spectroscopy, as synthesized PbSe QDs were dropcast onto Si windows from concentrated hexane solution. Next, the QD films were submerged in 1 mM EDT acetonitrile solution to remove most of the native oleate ligands, which have IR bands in the regions where we expected to see intraband transitions. Then, the EDT exchanged QD films were submerged in silver nitrate ethanol solutions for varying amounts of time to incorporate Ag^+ ions.

d. XRF Analysis

Films were prepared for XRF analysis by dropcasting undoped or solution doped Ag:PbSe QDs from hexane onto Si or FTO substrates.

E. Quantitative ^{1}H NMR

Quantitative ^{1}H NMR spectra were recorded on a Bruker Avance III 400 MHz instrument and acquired with sufficiently long delay to allow complete relaxation between pulses (30 s). Undoped and solution doped Ag:PbSe QDs were dispersed in $CDCl_3$. Surface bound oleate ligand density was estimated using a combination of UV-Vis-NIR and ^{1}H NMR spectra. First, the concentration of a TCE solution of corresponding QDs was standardized using UV-Vis-NIR absorbance at 400 nm. The addition of a known amount of ferrocene (10 H's) as an internal standard to the QD NMR sample allowed us to estimate the total number of surface bound oleate ligands using the well-resolved vinyl proton peak.

F. Electron Paramagnetic Resonance (EPR) Spectroscopy

EPR spectroscopy measurements were performed on a Bruker E500. Undoped and Ag:PbSe QD samples dispersed in anhydrous toluene or hexane, loaded into high purity 4 mm EPR tubes, and then sealed under nitrogen atmosphere. The system was calibrated to a weak pitch calibration standard, confirming instrument sensitivity to approximately 9×10^{12} spins. Measurements were performed at intermittent temperatures between ambient and 6 K. A closed loop helium cryostat was used to obtain cryogen temperatures. At each temperature we used 10 G modulation, varied the microwave power from 10 mW to 0.1mW, and scanned g-values from 1.5 to 2.2.

G. Elemental Analysis

a. Inductively Coupled Plasma – Mass Spectrometry (ICP-MS)

ICP-MS analysis was performed on an Agilent 7700 ICP-MS. Undoped and Ag:PbSe QD samples were digested using concentrated nitric acid and diluted with ultrapure water for analysis.

b. X-Ray Fluorescence (XRF) Spectroscopy

XRF spectroscopy was measured on a Fischerscope X-Ray XDV-SDD system equipped with a tungsten anode and a Peltier-cooled silicon drift detector. Undoped and Ag:PbSe QDs were drop cast from concentrated hexane suspensions onto a silicon substrate. The composition was quantified using the provided WinFTM software and the average of three measurements is reported per sample.

H. UV-Vis-NIR Absorption Spectroscopy

Ground state optical absorbance spectra of undoped and Ag:PbSe QD samples supended in TCE were collected using a Cary 500 UV-Vis-NIR spectrometer.

I. Photoluminescence quantum yield (PL QY) Spectroscopy

PL QY measurements for undoped and Ag:PbSe QD samples suspended in TCE were made using a previously established method.[42] QDs were dispersed in TCE with an absorbance of less than 0.1 OD at the excitation peak wavelength to minimize reabsorption effects. The measurements were taken in a LabSphere integration sphere with an 850 nm NIR-LED (ThorLabs M850L3) excitation source passed through an 850 nm centered 40 nm band-pass filter. Light from the sphere was fiber coupled to a home-built fluorescence spectrometer consisting of a 900 nm long-pass filter, monochromator (PTI), and a two-stage thermocouple-cooled extended InGaAs detector. The excitation LED was driven by a 15 V square wave at 25 Hz using a Stanford Research Systems (SRS) DS335 function generator. The detector signal was amplified using a SRS SR530 lock-in amplifier, and all spectra were corrector for grating, fiber, integration sphere, and detector deficiencies using a calibrated lamp. The PL QY was calculated using:

$$PL\ QY = \frac{\int I_{sample}(\lambda) - I_{ref}(\lambda)\, d\lambda}{\int E_{ref}(\lambda) - E_{sample}(\lambda)\, d\lambda}$$

where ‘I’ indicates the measured intensity of the emitted light, ‘E’ indicates the measured intensity of the excitation light, ‘sample’ indicates measurements of QD samples, and ‘ref’ indicates measurements of a reference cuvette (contains pure solvent, TCE, without QDs).

J. Fourier Transform – Infrared (FT-IR) Spectroscopy

FT-IR absorbance measurements were taken on a Thermo-Nicolet 6700 FT-IR spectrometer in transmission mode with a resolution of 4 cm^{-1}. Clean Si plates were sealed in a nitrogen filled glovebox and used for background measurements. Spectra with sloping baselines were baseline-corrected.

K. Transmission Electron Microscopy (TEM)

Transmission electron microscopy was performed using an FEI Tecnai G2 ST20 TEM operating at 200 kV. Samples were prepared by dropcasting undoped and solution doped Ag:PbSe QDs from dilute hexane solutions onto carbon coated copper grids.

L. X-Ray Diffraction (XRD)

X-ray diffraction (XRD) was performed on a Bruker D8 Discover diffractometer using Cu Kα radiation (λ =1.54 Å). For high resolution experiments, QD samples were dropcast on FTO substrates, which simultaneously served as reflection peak references, and encapsulated using Kapton tape. In order to reduce error in the peak positions tilt correction from sample to sample was done by using the FTO peaks as a reference. Deconvolution for the high resolution data included both the Kα1 and Kα2 lines by fitting the following function:

$$f(x) = 2A_{K\alpha 2} * Exp(\frac{x-x_0}{w})^2 + \ A_{K\alpha 2} * Exp(\frac{x-(x_0+offset)}{w})^2$$

Where $A_{k\alpha 2}$ is the intensity due to the $K_{\alpha 2}$ line (the $K_{\alpha 1}$ line is twice the amplitude of the $K_{\alpha 2}$ line), w is the Gaussian width and the offset is the difference between the $K_{\alpha 1}$ and $K_{\alpha 2}$ lines which is angle dependent.

M. Photoelectron Spectroscopy

PES measurements were performed on a Physical Electronics, Inc. 5600 ESCA instrument, which has been discussed in detail previously.[43] Briefly, the XPS radiation is produced by a monochromatic Al (Kα) source centered at 1486.6 eV. The valence band spectra were taken with a step size of 0.05 eV and a pass energy of 5.85 eV. The electron binding energy scale was calibrated using the Fermi edge of cleaned metallic substrates (Au, Mo, Cu, and/or Ag), giving the spectra an uncertainty of ±0.05 eV. UPS measurements (He (Iα) = 21.22 eV) were taken with a step size of 0.025 eV and a pass energy of 2.95 eV. The calibrations were done on the same cleaned substrates giving an energy uncertainty of ±0.025 eV.

The correction to the extracted onset of photoelectron intensity needed to better approximate the $(E_F - E_{VBM})$ value of Ag:PbSe QDs has been previously discussed by Miller *et al.*[28] Briefly, the correction depends on the band gap (E_g = optical band gap + exciton binding energy); the correction to the onset of photoelectron intensity is *correction = 0.382 - 0.226(E_g).* For this study, the optical band gap and exciton binding energy of the native PbSe QD is 0.86 and 0.03 eV, respectively, which gives E_g = 0.89 eV and a correction of 0.181 eV. Therefore, $(E_F - E_{VBM})$ = $(E_F - E_{onset})$ – (0.181 eV) for the PbSe QD films used in this study.

N. Transient Absorption (TA)

Femtosecond TA spectra were collected using a home-built instrument. A Continuum Integra-C regeneratively amplified Ti:sapphire laser with ~3.5 W, 1 kHz, and ~100 fs pulse width output at 800 nm is split into two beams; pump and probe. The pump beam is directed into a Palitra-Duo-FS:FS optical parametric amplifier that is capable of producing excitation wavelengths from 270-22,000 nm and is modulated at 500 Hz through an optical chopper to block every other laser pulse. The probe beam passes through a multipass delay stage that can achieve up to ~4.5 ns of pump-probe delay and is focused onto a sapphire crystal to produce a broadband Vis-NIR spectrum from 800-1600 nm. The probe is passed through a continuously variable neutral density filter and a fraction is separated off to be used as a reference that accounts for probe beam intensity fluctuations. The pump and probe beams are then overlapped at the sample, which is vigorously stirred to eliminate photocharging effects. NIR photodiode arrays (Ultrafast Systems) are used to detect the probe and reference beams for data acquisition.

Sub-nanosecond TA measurements were performed using an Ultrafast Systems LLC EOS Spectrometer.

O. $k \cdot p$ Theory Calculations

Isotropic $k \cdot p$ four-band envelope function formalism calculations were performed following Kang *et al.*[44] Using reported literature values of oleate capped PbSe QD bandgaps versus QD core diameter, we apply a constant correction factor to the QD diameter in the calculations to better model the physical boundary conditions of the QD core.[45,46]

▪ *Associated Content*

Supporting Information High-resolution x-ray diffraction data, ^{1}H NMR spectroscopy data, control absorbance measurements, and photoelectron spectroscopy data.

▪ *Author Information*

Corresponding Author
* matt.beard@nrel.gov

Author Contributions

ǂ Authors contributed equally to this work

ORCID

Daniel M. Kroupa: 0000-0002-2788-3670
Matthew C. Beard: 0000-0002-2711-1355

Notes

The authors declare no competing financial interest.

▪ *Acknowledgements*

The authors would like to thank Dave Bobela for help with EPR experiments. D.M.K, B.K.H, E.M.M., N.C.A., and M.C.B. respectfully acknowledge support through the Division of Chemical Sciences, Geosciences and Biosciences, Office of Basic Energy Sciences, Office of Science within the US Department of Energy. B.D.C was supported as part of the Center for Advanced Solar Photophysics, an Energy Frontier Research Center funded by the Office of Basic Energy Sciences, Office of Science with DOE. D.T.M. acknowledge the NREL Director's Fellowship Program. Work at NREL was performed under contract No. DE-AC36-08GO28308 from DOE.

▪ *References*

(1) Shklovskii, B. I.; Efros, A. L. *Electronic Properties of Doped Semiconductors*; Springer Science & Business Media: Berlin, 2013.

(2) Engel, J. H.; Surendranath, Y.; Alivisatos, A. P. Controlled Chemical Doping of Semiconductor Nanocrystals Using Redox Buffers. *J. Am. Chem. Soc.* **2012**, *134*, 13200–13203.

(3) Koh, W.; Koposov, A. Y.; Stewart, J. T.; Pal, B. N.; Robel, I.; Pietryga, J. M.; Klimov, V. I. Heavily Doped N-Type PbSe and PbS Nanocrystals Using Ground-State Charge Transfer from Cobaltocene. *Sci. Rep.* **2013**, *3*, 1–8.

(4) Shim, M.; Guyot-Sionnest, P. N-Type Colloidal Semiconductor Nanocrystals. *Nature* **2000**, *407*, 981–983.

(5) Rinehart, J. D.; Schimpf, A. M.; Weaver, A. L.; Cohn, A. W.; Gamelin, D. R. Photochemical Electronic Doping of Colloidal CdSe Nanocrystals. *J. Am. Chem. Soc.* **2013**, *135*, 18782–18785.

(6) Wehrenberg, B. L.; Guyot-Sionnest, P. Electron and Hole Injection in PbSe Quantum Dot Films. *J. Am. Chem. Soc.* **2003**, *125*, 7806–7807.

(7) Wang, C.; Shim, M.; Guyot-Sionnest, P. Electrochromic Nanocrystal Quantum Dots. *Science* **2001**, *291*, 2390–2392.

(8) Liu, H.; Keuleyan, S.; Guyot-Sionnest, P. N- and P-Type HgTe Quantum Dot Films. *J. Phys. Chem. C* **2012**, *116*, 1344–1349.

(9) Schimpf, A. M.; Knowles, K. E.; Carroll, G. M.; Gamelin, D. R. Electronic Doping and Redox-Potential Tuning in Colloidal Semiconductor Nanocrystals. *Acc. Chem. Res.* **2015**, *48*, 1929–1937.

(10) Galli, G. Solid-State Physics: Doping the Undopable. *Nature* **2005**, *436*, 32–33.

(11) Erwin, S. C.; Zu, L.; Haftel, M. I.; Efros, A. L.; Kennedy, T. A.; Norris, D. J. Doping Semiconductor Nanocrystals. *Nature* **2005**, *436*, 91–94.

(12) Wang, S.; Zheng, G.; Luo, T.; She, X.; Li, H.; Tang, X. Exploring the Doping Effects of Ag in P-Type PbSe Compounds with Enhanced Thermoelectric Performance. *J. Phys. Appl. Phys.* **2011**, *44*, 475304.

(13) Buonsanti, R.; Milliron, D. J. Chemistry of Doped Colloidal Nanocrystals. *Chem. Mater.* **2013**, *25*, 1305–1317.

(14) Mocatta, D.; Cohen, G.; Schattner, J.; Millo, O.; Rabani, E.; Banin, U. Heavily Doped Semiconductor Nanocrystal Quantum Dots. *Science* **2011**, *332*, 77–81.

(15) Sahu, A.; Kang, M. S.; Kompch, A.; Notthoff, C.; Wills, A. W.; Deng, D.; Winterer, M.; Frisbie, C. D.; Norris, D. J. Electronic Impurity Doping in CdSe Nanocrystals. *Nano Lett.* **2012**, *12*, 2587–2594.

(16) Kang, M. S.; Sahu, A.; Frisbie, C. D.; Norris, D. J. Influence of Silver Doping on Electron Transport in Thin Films of PbSe Nanocrystals. *Adv. Mater.* **2013**, *25*, 725–731.

(17) Stavrinadis, A.; Rath, A. K.; de Arquer, F. P. G.; Diedenhofen, S. L.; Magén, C.; Martinez, L.; So, D.; Konstantatos, G. Heterovalent Cation Substitutional Doping for Quantum Dot Homojunction Solar Cells. *Nat. Commun.* **2013**, *4*, 2981.

(18) Stavrinadis, A.; Pelli Cresi, J. S.; D'Acapito, F.; Magen, C.; Boscherini, F.; Konstantatos, G. Aliovalent Doping in Colloidal Quantum Dots and Its Manifestation on Their Optical Properties: Surface Attachment versus Structural Incorporation. *Chem. Mater.* **2016**, *28*, 5384–5393.

(19) Choi, H.; Ko, J.-H.; Kim, Y.-H.; Jeong, S. Steric-Hindrance-Driven Shape Transition in PbS Quantum Dots: Understanding Size-Dependent Stability. *J. Am. Chem. Soc.* **2013**, *135*, 5278–5281.

(20) Owen, J. The Coordination Chemistry of Nanocrystal Surfaces. *Science* **2015**, *347*, 615–616.

(21) Moreels, I.; Lambert, K.; De Muynck, D.; Vanhaecke, F.; Poelman, D.; Martins, J. C.; Allan, G.; Hens, Z. Composition and Size-Dependent Extinction Coefficient of Colloidal PbSe Quantum Dots. *Chem. Mater.* **2007**, *19*, 6101–6106.

(22) Anderson, N. C.; Hendricks, M. P.; Choi, J. J.; Owen, J. S. Ligand Exchange and the Stoichiometry of Metal Chalcogenide Nanocrystals: Spectroscopic Observation of Facile Metal-Carboxylate Displacement and Binding. *J. Am. Chem. Soc.* **2013**, *135*, 18536–18548.

(23) An, J. M.; Franceschetti, A.; Zunger, A. Pauli Blocking versus Electrostatic Attenuation of Optical Transition Intensities in Charged PbSe Quantum Dots. *Phys. Rev. B* **2007**, *76*, 161310.

(24) Luther, J. M.; Jain, P. K.; Ewers, T.; Alivisatos, A. P. Localized Surface Plasmon Resonances Arising from Free Carriers in Doped Quantum Dots. *Nat. Mater.* **2011**, *10*, 361–366.

(25) Sahu, A.; Qi, L.; Kang, M. S.; Deng, D.; Norris, D. J. Facile Synthesis of Silver Chalcogenide (Ag2E; E = Se, S, Te) Semiconductor Nanocrystals. *J. Am. Chem. Soc.* **2011**, *133*, 6509–6512.

(26) Sahu, A.; Khare, A.; Deng, D. D.; Norris, D. J. Quantum Confinement in Silver Selenide Semiconductor Nanocrystals. *Chem. Commun.* **2012**, *48*, 5458–5460.

(27) Oh, S. J.; Berry, N. E.; Choi, J.-H.; Gaulding, E. A.; Paik, T.; Hong, S.-H.; Murray, C. B.; Kagan, C. R. Stoichiometric Control of Lead Chalcogenide Nanocrystal Solids to Enhance Their Electronic and Optoelectronic Device Performance. *ACS Nano* **2013**, *7*, 2413–2421.

(28) Miller, E. M.; Kroupa, D. M.; Zhang, J.; Schulz, P.; Marshall, A. R.; Kahn, A.; Lany, S.; Luther, J. M.; Beard, M. C.; Perkins, C. L.; *et al.* Revisiting the Valence and Conduction Band Size Dependence of PbS Quantum Dot Thin Films. *ACS Nano* **2016**, *10*, 3302–3311.

(29) Kohn, S. E.; Yu, P. Y.; Petroff, Y.; Shen, Y. R.; Tsang, Y.; Cohen, M. L. Electronic Band Structure and Optical Properties of PbTe, PbSe, and PbS. *Phys. Rev. B* **1973**, *8*, 1477–1488.

(30) Zembutsu, S. X-ray Photoelectron Spectroscopy Studies of Ag Photodoping in Se-Ge Amorphous Films. *Appl. Phys. Lett.* **1981**, *39*, 969–971.

(31) Zhang, J.; Chernomordik, B. D.; Crisp, R. W.; Kroupa, D. M.; Luther, J. M.; Miller, E. M.; Gao, J.; Beard, M. C. Preparation of Cd/Pb Chalcogenide Heterostructured Janus Particles via Controllable Cation Exchange. *ACS Nano* **2015**, *9*, 7151–7163.

(32) Smith, D. K.; Luther, J. M.; Semonin, O. E.; Nozik, A. J.; Beard, M. C. Tuning the Synthesis of Ternary Lead Chalcogenide Quantum Dots by Balancing Precursor Reactivity. *ACS Nano* **2011**, *5*, 183–190.

(33) Kubaschewski, O.; Effenberg, G. *Ag-Pb-Se Ternary Phase Diagram Evaluation · Phase Diagrams, Crystallographic and Thermodynamic Data*; 10.10884.1.9; MSI Materials Science International Services GmbH: Stuttgart, 1988.

(34) Seltzer, M. S.; Jr, J. B. W. Self-Diffusion of Lead-210 in Single Crystals of Lead Selenide. *J. Chem. Phys.* **1962**, *36*, 130–134.

(35) Hughes, B. K.; Ruddy, D. A.; Blackburn, J. L.; Smith, D. K.; Bergren, M. R.; Nozik, A. J.; Johnson, J. C.; Beard, M. C. Control of PbSe Quantum Dot Surface Chemistry and Photophysics Using an Alkylselenide Ligand. *ACS Nano* **2012**, *6*, 5498–5506.

(36) Fedorovich, N. A. Diffusion of Silver and Sodium in Lead Selenide. *Sov. Phys.-Solid State* **1965**, *7*, 1593.

(37) Amit, Y.; Li, Y.; Frenkel, A. I.; Banin, U. From Impurity Doping to Metallic Growth in Diffusion Doping: Properties and Structure of Silver-Doped InAs Nanocrystals. *ACS Nano* **2015**, *9*, 10790–10800.

(38) Peng, H.; Song, J.-H.; Kanatzidis, M. G.; Freeman, A. J. Electronic Structure and Transport Properties of Doped PbSe. *Phys. Rev. B* **2011**, *84*, 125207.

(39) Cragg, G. E.; Efros, A. L. Suppression of Auger Processes in Confined Structures. *Nano Lett.* **2010**, *10*, 313–317.

(40) Efros, A. L.; Nesbitt, D. J. Origin and Control of Blinking in Quantum Dots. *Nat. Nanotechnol.* **2016**, *11*, 661–671.

(41) Moreels, I.; Fritzinger, B.; Martins, J. C.; Hens, Z. Surface Chemistry of Colloidal PbSe Nanocrystals. *J. Am. Chem. Soc.* **2008**, *130*, 15081–15086.

(42) Semonin, O. E.; Johnson, J. C.; Luther, J. M.; Midgett, A. G.; Nozik, A. J.; Beard, M. C. Absolute Photoluminescence Quantum Yields of IR-26 Dye, PbS, and PbSe Quantum Dots. *J. Phys. Chem. Lett.* **2010**, *1*, 2445–2450.

(43) Perkins, C. L.; Hasoon, F. S. Surfactant-Assisted Growth of CdS Thin Films for Photovoltaic Applications. *J. Vac. Sci. Technol. A* **2006**, *24*, 497–504.

(44) Kang, I.; Wise, F. W. Electronic Structure and Optical Properties of PbS and PbSe Quantum Dots. *J. Opt. Soc. Am. B* **1997**, *14*, 1632.

(45) Norris, D. J.; Bawendi, M. G. Measurement and Assignment of the Size-Dependent Optical Spectrum in CdSe Quantum Dots. *Phys. Rev. B* **1996**, *53*, 16338–16346.

(46) Diaconescu, B.; Padilha, L. A.; Nagpal, P.; Swartzentruber, B. S.; Klimov, V. I. Measurement of Electronic States of PbS Nanocrystal Quantum Dots Using Scanning Tunneling Spectroscopy: The Role of Parity Selection Rules in Optical Absorption. *Phys. Rev. Lett.* **2013**, *110*, 127406.

- ***TOC Graphic***

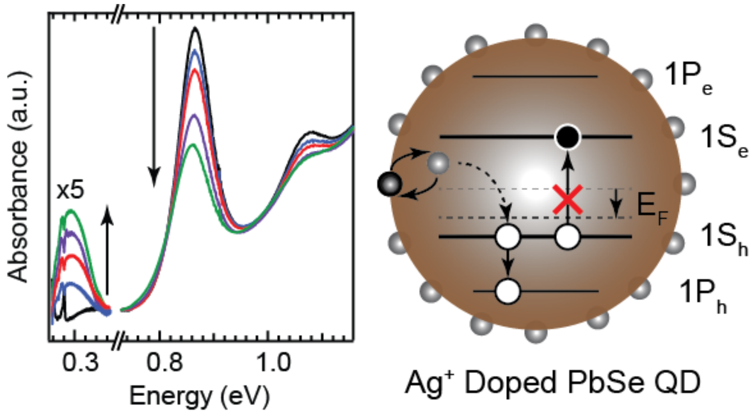
Absorbance (a.u.)
x5
0.3
0.8
1.0
Energy (eV)
1P$_e$
1S$_e$
E$_F$
1S$_h$
1P$_h$
Ag$^+$ Doped PbSe QD

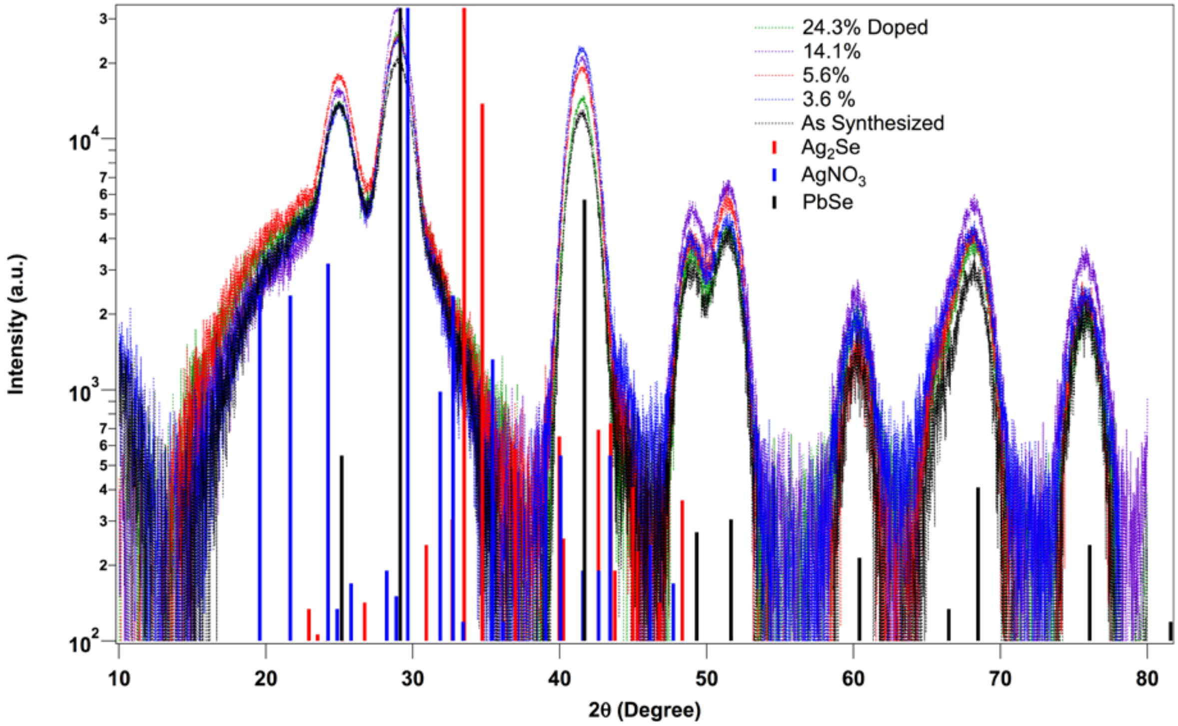

Figure S1. Log plot of XRD data (Fig. 1C) showing no evidence of the formation of either Ag_2Se or AgNO3. Shifting of the the XRD peaks (consistent with a reduction of the PbSe lattice parameter upon alloying with Ag) should result in ~ 0.2 degree shift of the line at 68 degrees for ~ 2% substitution of Pb with Ag . However, this is within the noise of the XRD data presented above.

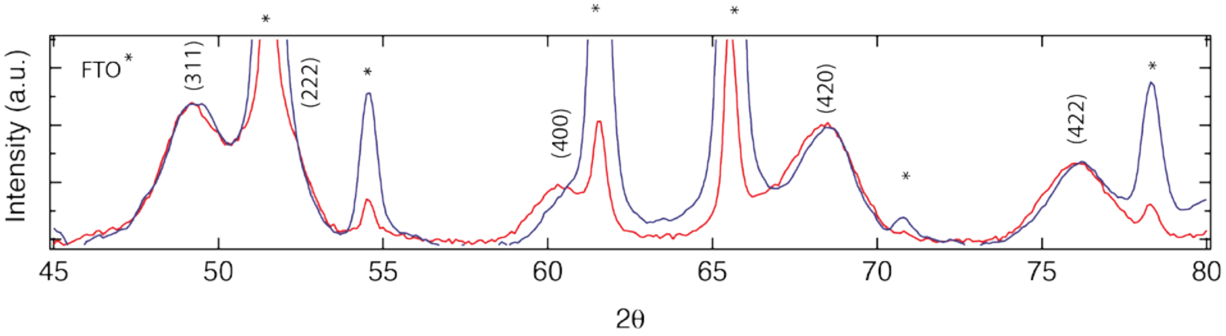

Figure S2. High resolution XRD scan of the undoped (red trace) and ~ 30% doped (blue trace) PbSe QDs deposited onto FTO/glass substrates. The FTO peaks (denoted by *) serve as a reference to calibrate the two spectra. Gaussian peak fitting function is employed to decouple the FTO peaks from the PbSe peaks; PbSe peak locations are found using a custom fit function described in the Methods Section. The best fit peak positions are tabulated below.

Table S1. Peak assignments and analysis of the high resolution XRD scans of undoped and Ag doped PbSe QD films shown in Figure S2. The entries with asterisks are inside the error due to strong overlap of the (222) and (311) PbSe peaks and the FTO peak at 51.5 degrees

Peak Identity	Peak Position	Error (+/-)
PbSe (422) undoped	76.22	0.022
PbSe (422) doped	76.39	0.053
PbSe (420) undoped	68.74	0.007
PbSe (420) doped	69.05	0.024
PbSe (400) – undoped	60.83	0.023
PbSe (400) - doped	61.82	0.042
*PbSe (222) – undoped	51.85	0.010
*PbSe (222) – doped	51.81	0.038
*PbSe (311) - undoped	49.42	0.063
*PbSe (311) – doped	49.34	0.053
PbSe (220) -- undoped	41.85	0.002
PbSe (220) -- doped	41.90	0.008

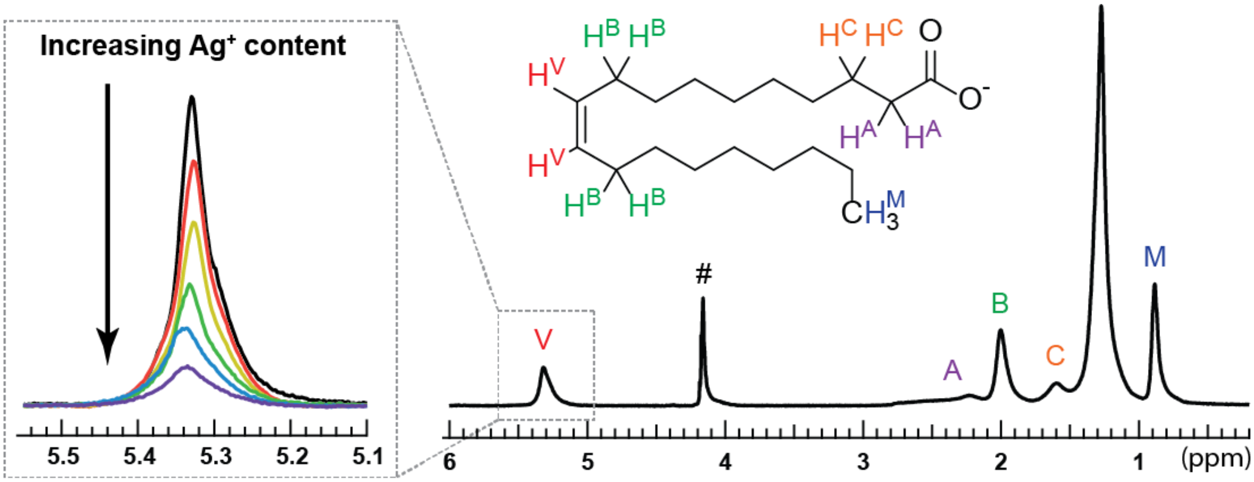

Figure S3. ^{1}H NMR spectrum of as synthesized 4.7 nm PbSe QDs in $CDCl_3$ with chemical shift assignments and a color coded, labeled oleate molecule for reference. The '#' symbol indicates the peak associated with our internal standard, ferrocene, which is used to quantify the number of oleate molecules in the sample. The panel on the left shows a magnified view of the oleate vinyl proton, H^V, region of the Ag doped PbSe QD samples normalized to the ferrocene peak. The QD concentration is slightly different for each sample, but, the overall decrease in NMR peak intensity suggests displacement of oleate from the QD surface with increasing Ag^+ content, as measured by XRF. A summary of the complete, quantitative analysis is detailed in Fig. 2 of the main text.

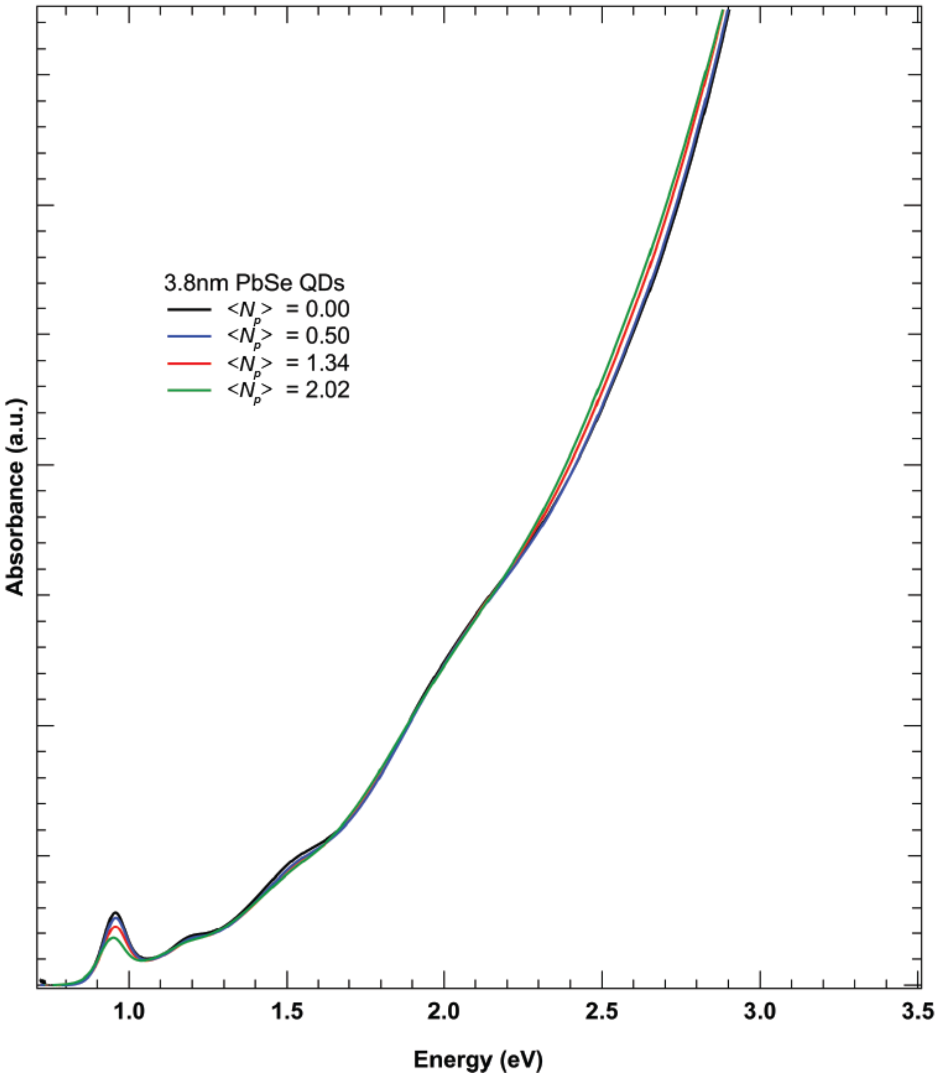

Figure S4. Absorbance spectra for 3.8 nm PbSe QDs with increasing Ag^+ incorporation.

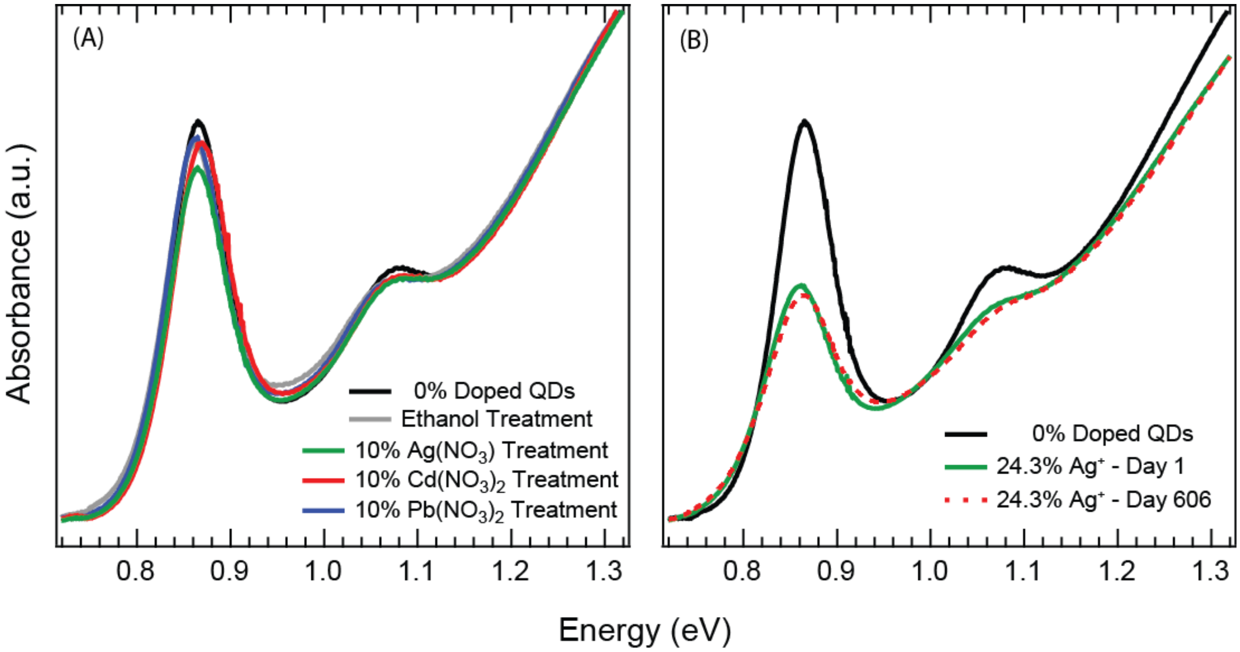

Figure S5. Control absorbance experiments of 4.7nm PbSe QD solutions. (A) The addition of Cd(NO$_3$)$_2$ (red), Pb(NO$_3$)$_2$ (blue), or neat ethanol (gray) results in moderate bleaching and shifting of the PbSe QD first exciton peak compared to the addition of Ag(NO$_3$) (green). (B) The absorbance spectrum of 4.7nm PbSe QDs with 24.3% Ag$^+$ incorporation exhibits nominal changes over 606 days of storage as a powder under inert atmosphere in the dark.

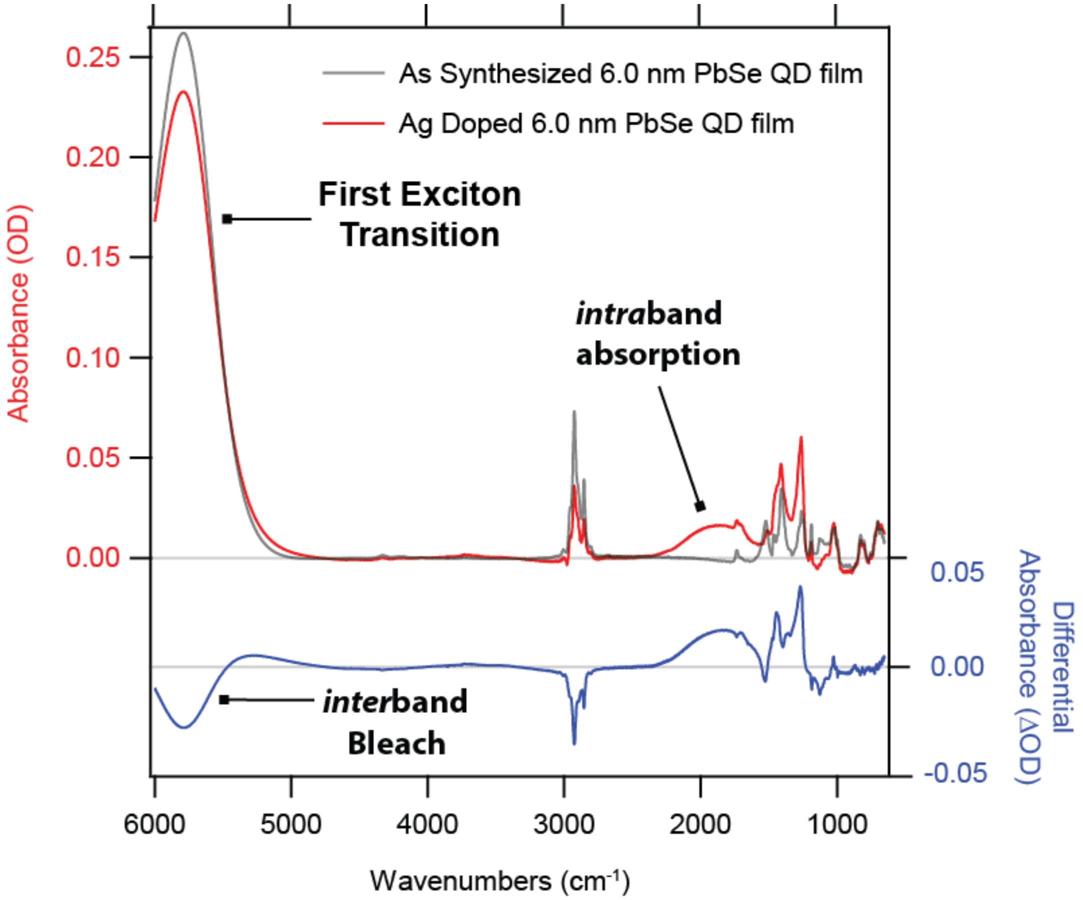

Figure S6. Reconstructed FT-IR absorbance spectrum for 6.0 nm EDT ligand exchanged Ag:PbSe QD film (red) from the undoped FT-IR absorbance spectrum (gray) and the differential absorbance spectrum with Ag^{+} incorporation (blue).

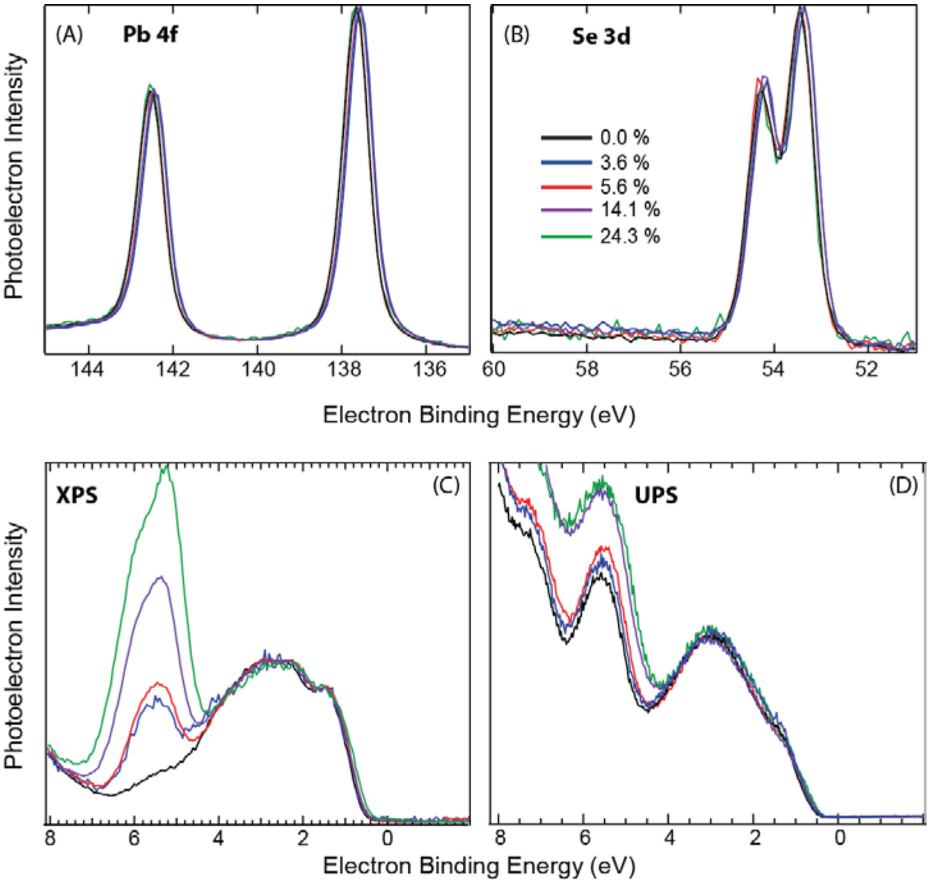

Figure S7. Photoelectron spectra for films of as synthesized (black), 3.6% Ag^+ doped (blue), 5.6% Ag^+ doped (red), 14.1% Ag^+ doped (purple), and 24.3% Ag^+ doped (green) 4.7 nm diameter PbSe QDs treated with EDT. Color coding for all panels follows the legend in panel (B). High-resolution XPS core level spectra of (A) Pb *4f* and (B) Se *3d* for PbSe QDs with different amounts of Ag^+ incorporation. The spectra show that with the addition of Ag^+, the peaks slightly shift to higher binding energy, which is consistent with p-type doping. There are no additional features that grow in with the addition of Ag^+, suggesting minimal or no oxidation of the QD films. Panel (C) and (D) show the broadband XPS and UPS spectra, respectively. In both (C) and (D), there is a noticeable increase in the photoelectron intensity around 5.5 eV with increasing Ag^+ content, which is due to photodetachment from the Ag *4d* orbital and is consistent with the formation of Ag-Se bonds.

Table S2. XPS and UPS results for films of 4.7 nm diameter PbSe QDs treated with EDT; atomic ratios, $(E_F - E_{VBM})$, and work function (Φ). Energies are reported in eV. UPS and Φ have an energy uncertainty of ±25 meV and XPS has an energy uncertainty of ±50 meV.

% Ag^+	$\langle N_p \rangle$	Pb:Se	Ag:Se	$(E_F - E_{VBM})$UPS	$(E_F - E_{VBM})$XPS	Φ
0.0	0.00	1.58	0.00	0.40	0.39	4.89
3.6	0.36	1.53	0.06	0.34	0.34	4.89
5.6	0.87	1.48	0.05	0.30	0.32	4.89
14.1	1.86	1.46	0.16	0.27	0.34	4.95
24.3	2.49	1.39	0.32	0.23	0.26	4.88

(1) Starting PbSe QD Composition / Dopant Addition

$[Pb^{2+}Se^{2-}]\ [PbSe]_{core}\ [Pb^{2+}(OA^{-})_2]_{surface} + Ag^{+}NO_3^{-}$

(2) Surface adsorption / Z-type ligand exchange

$[Pb^{2+}Se^{2-}]\ [PbSe]_{core}\ [Ag^{+}NO_3^{-}]_{surface} + Pb^{2+}(OA^{-})_2$

(3) Ag^{+} lattice incorporation / Ag-Se hybrid acceptor level Formation

$[Ag^{+}Se^{2-}]\ [PbSe]_{core}\ [Pb^{2+}NO_3^{-}]_{surface} + Pb^{2+}(OA^{-})_2$